Monitoring and modeling dispersal of a submerged nearshore berm at the mouth of the Columbia River, USA

Stevens, Andrew W.; Moritz, Hans R.; Elias, Edwin P.L.; Gelfenbaum, Guy R.; Ruggiero, Peter R.; Pearson, Stuart G.; McMillan, James M.; Kaminsky, George M.

DOI
10.1016/j.coastaleng.2023.104285

Publication date
2023

Document Version
Final published version

Published in
Coastal Engineering

Citation (APA)
Stevens, A. W., Moritz, H. R., Elias, E. P. L., Gelfenbaum, G. R., Ruggiero, P. R., Pearson, S. G., McMillan, J. M., & Kaminsky, G. M. (2023). Monitoring and modeling dispersal of a submerged nearshore berm at the mouth of the Columbia River, USA. *Coastal Engineering*, *181*, Article 104285. https://doi.org/10.1016/j.coastaleng.2023.104285

Coastal Engineering 181 (2023) 104285

Contents lists available at ScienceDirect

Coastal Engineering

journal homepage: www.elsevier.com/locate/coastaleng

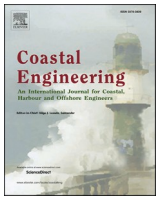

Monitoring and modeling dispersal of a submerged nearshore berm at the mouth of the Columbia River, USA

Andrew W. Stevens [a,*], Hans R. Moritz [b], Edwin P.L. Elias [c], Guy R. Gelfenbaum [a], Peter R. Ruggiero [d], Stuart G. Pearson [c,e], James M. McMillan [b], George M. Kaminsky [f]

[a] U.S. Geological Survey, Pacific Coastal and Marine Science Center, 2885 Mission St., Santa Cruz, CA, 95060, USA
[b] U.S. Army Corps of Engineers, Portland District, 333 SW First Ave, Portland, OR, 97204, USA
[c] Deltares, P.O. Box 177, 2600 MH, Delft, the Netherlands
[d] Oregon State University, College of Earth, Ocean, and Atmospheric Sciences, 2651 SW Orchard Avenue, Corvallis, OR, 97331, USA
[e] Delft University of Technology, Faculty of Civil Engineering and Geosciences, P.O. Box 5048, 2600GA, Delft, the Netherlands
[f] Washington State Department of Ecology, Coastal Monitoring and Analysis Program, P.O. Box 47600, Olympia, WA, 98504-7600, USA

ARTICLE INFO

Keywords:
Nearshore berm
Process-based modeling
Delft3D
Sediment transport

ABSTRACT

A submerged, low-relief nearshore berm was constructed in the Pacific Ocean near the mouth of the Columbia River, USA, using 216,000 m^3 of sediment dredged from the adjacent navigation channel. The material dredged from the navigation channel was placed on the northern flank of the ebb-tidal delta in water depths between 12 and 15 m and created a distinct feature that could be tracked over time. Field measurements and numerical modeling were used to evaluate the transport pathways, time scales, and physical processes responsible for dispersal of the berm and evaluate the suitability of the location for operational placement of dredged material to enhance the sediment supply to eroding beaches onshore of the placement site. Repeated multibeam bathymetric surveys characterized the initial berm morphology and dispersion of the berm between September 22, 2020, and March 10, 2021. During this time, the volume of sediment within the berm decreased by about 40%to 127,000 m^3, the maximum height decreased by almost 60%, and the center of the deposit shifted onshore over 200 m. Observations of berm morphology were compared with predictions from a three-dimensional hydrodynamic and sediment transport model application to refine poorly constrained model input parameters including sediment transport coefficients, bed schematization, and grain size. The calibrated sediment transport model was used to predict the amount, timing, and direction of transport outside of the observed survey area. Model simulations predicted that tidal currents were weak in the vicinity of the berm and wave processes including enhanced bottom stresses and asymmetric bottom orbital velocities resulted in dominant onshore movement of sediment from the berm toward the coastline. Roughly 50% of the berm volume was predicted to disperse away from the initial placement site during the 169 day hindcast. Between 9 and 17% of the initial volume of the berm was predicted to accumulate along the shoreface of a shoreline reach experiencing chronic erosion directly onshore of the placement site. Scenarios exploring alternate placement locations suggested that the berm was relatively effective in enhancing the sediment supply along the eroding coastline north of the inlet. The transferable monitoring and modeling framework developed in this study can be used to inform implementation of strategic nearshore placements and regional sediment management in complex, high-energy coastal environments elsewhere.

1. Introduction

Inlets throughout the world are commonly engineered to improve navigation using a combination of jetty construction and maintenance dredging of channels. These engineering projects can alter sediment transport pathways (Kaminsky et al., 2010) and often lead to morphological change along adjacent beaches (Houston and Dean, 2016), especially when dredged material is disposed offshore and removed from the littoral system. Beach nourishment is one approach to beneficially utilize sediment dredged from navigation channels to restore and

* Corresponding author.
E-mail address: astevens@usgs.gov (A.W. Stevens).

https://doi.org/10.1016/j.coastaleng.2023.104285
Received 18 March 2022; Received in revised form 2 November 2022; Accepted 20 January 2023
Available online 23 January 2023

enhance sediment supply and reduce coastal erosion impacts (de Schipper et al., 2021). Monitoring and modeling of both large (e.g., Luijendijk et al., 2017) and small (e.g., Yates et al., 2009) projects suggest that beach nourishment can successfully mitigate coastal erosion impacts. Although the volume of sediment placed in beach nourishments has increased exponentially in the U.S. (Elko et al., 2021), high costs, logistical and regulatory challenges, and environmental concerns (e.g., Schlacher et al., 2012) often limit the ability to nourish beaches directly.

Strategic placement of sediment in the active nearshore is another approach to nourish beaches indirectly whereby natural processes transport a portion of the sediment from the placement site to desired onshore locations (Gailani et al., 2019). Reduced costs, decreased disruption to public access, and lessened impacts on fragile coastal habitats are factors that make strategic nearshore placement a desirable alternative to beach nourishment. However, careful consideration of the spatial and temporal distribution of sediment fluxes and morphological change is required to select effective placement areas and determine volumes needed to achieve the desired outcomes of strategic placement projects. Previous field observations and numerical modeling studies that have evaluated strategic placements in both high- and low-energy environments inform current practices (Mendes et al., 2021; Brutsche et al., 2014; Huisman et al., 2019), but the complexity in physical processes and wide variety of coastal landforms often require site-specific predictions of sediment transport to optimize dredged material management strategies.

Despite recent advances in numerical modeling and increased computing capacity (e.g., Luijendijk et al., 2017; Bertin et al., 2020; Roelvink et al., 2020), prediction of sediment transport and morphology change in coastal settings at spatial and temporal scales sufficient to inform regional sediment management remains challenging (French et al., 2016). Uncertainty in predictions of sediment transport from parameterization of important physical processes (e.g., Albernaz et al., 2019), schematization of the computational grid (horizontal resolution, vertical layering in water column and seabed), and uncertainty or simplification of model input parameters affect predictions of transport fluxes and can alter predicted transport pathways (Allen et al., 2021). Field data from a variety of coastal settings are therefore critical to test, improve, and understand the limitations of model predictions for use in sediment management decisions (Ludka et al., 2019, van Prooijen et al., 2020).

In this study, a combination of field measurements and numerical modeling was used to improve understanding and prediction of coastal processes and to inform regional sediment management at the mouth of the Columbia River, USA. Repeated bathymetric surveys were performed to document the creation and near-field dispersion of a submerged nearshore berm composed of sediment dredged from the navigation channel and placed north of the inlet. Observations of the berm morphology were compared against predictions from a three-dimensional (3D) hydrodynamic and sediment transport model and model predictions were calibrated based on variations in transport-formula coefficients, sediment grain size, and bed schematization parameters. Model simulations predicted the fate of berm sediment for approximately 6 months following placement and a range of scenarios were used to investigate alternative locations for strategic placements of

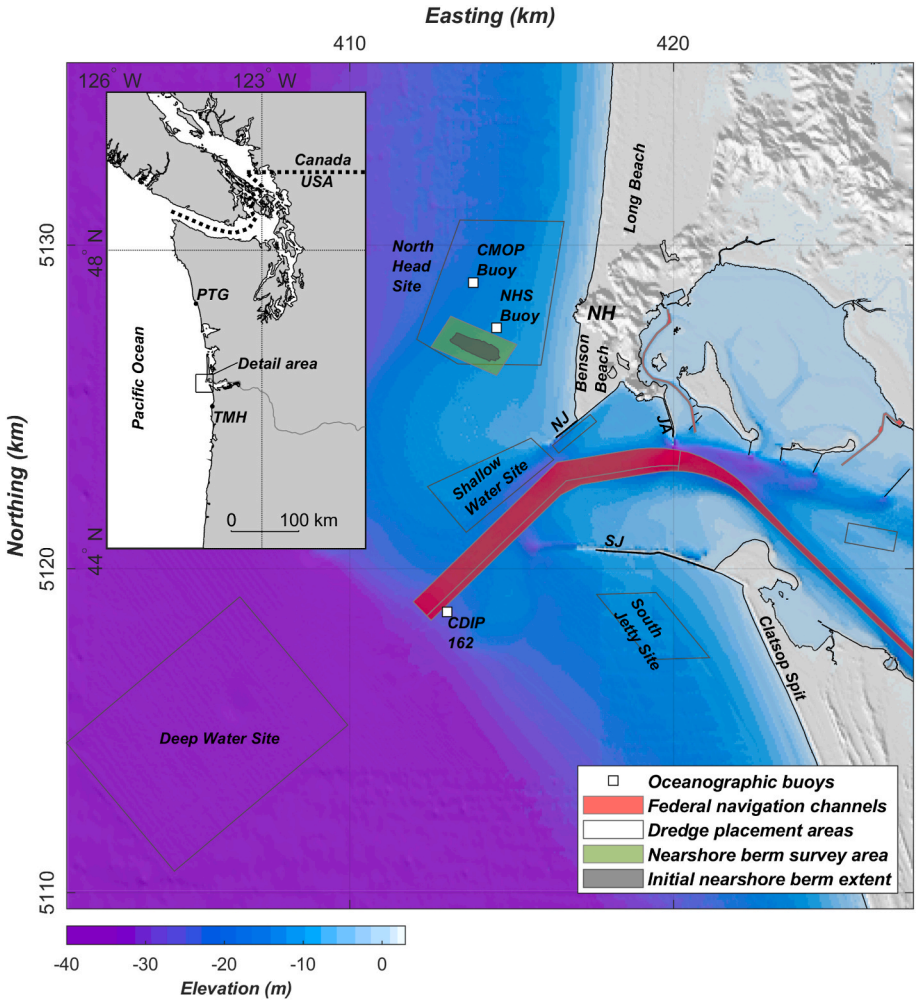

Fig. 1. Map of the mouth of the Columbia River study area showing locations of observational buoys used for model validation, dredge placement areas (black polygons), maintained federal navigation channels (red polygons), survey area of the nearshore berm (green box) within the North Head Site, and initial extent of the berm after placement. Also shown are the locations of the North Jetty (NJ), South Jetty (SJ), Jetty A (JA), North Head (NH), Tillamook Head (TMH), and Point Grenville (PTG).

dredged sediment. Combined, these techniques allow for quantification of the amount, timing, and dominant processes responsible for transport of sediment between the dredge placement sites on the ebb tidal delta and onshore beaches. The improved understanding and capacity to predict sediment transport processes is applied to optimize beneficial use of dredged material in a high energy coastal system.

2. Study Area

The Columbia River has historically been the primary source of sediment to approximately 165 km of shoreline between Point Grenville, Washington, and Tillamook Head, Oregon (Fig. 1). The Columbia River discharges into the Eastern North Pacific Ocean at the border of Oregon and Washington States. The Eastern North Pacific is characterized by an extremely energetic wave climate (Ahn et al., 2022), where winter storms regularly generate significant wave heights that are greater than 10 m and strong seasonal variations result in mean average wave heights of approximately 3.8 and 1.6 m for winter and summer, respectively (Ruggiero et al., 2010). Within the mesotidal Columbia River inlet, waves and estuarine circulation associated with major freshwater inputs modify the flow and sediment transport fields (Elias and Gelfenbaum, 2009). Ocean tides are classified as mixed semi-diurnal with a mean tidal range of 2.1 m (NOAA station 9439040).

The U.S. Army Corps of Engineers (USACE) maintains the Columbia-Snake River navigation system, which extends upstream 756 km from the entrance at the Pacific Ocean. The federal navigation channel at the mouth of the Columbia River is the gateway to this system, and is maintained with annual dredging, training dikes, and three major stone jetties (Fig. 1), originally constructed between 1885 and 1939. The Columbia River North (NJ) and South Jetties (SJ) extend approximately 3.5 and 10 km seaward, respectively, while Jetty A (JA) is slightly inside of the inlet and orthogonal to the channel axis. The construction of the jetties altered hydrodynamic processes, transport pathways, and sediment supplies resulting in increased rates of shoreline progradation for several decades along much of the Columbia River littoral cell (Kaminsky et al., 2010). Although progradation along the Columbia River littoral cell continues today (Ruggiero et al., 2016; Stevens et al., 2020), beach erosion has been observed at several locations including Benson Beach, a 3-km stretch of coastline immediately north of the North Jetty. Erosion along Benson Beach has been problematic for decades, with an average rate of shoreline retreat of 8.2 m/yr between the 1950s and 1999 (Kaminsky et al., 2010). Over 2 Mm^3 of sand eroded from Benson Beach and adjacent nearshore areas between 2014 and 2019 (Stevens et al., 2020). Persistent erosion along Benson threatens the stability of the North Jetty and has prompted various interventions including onshore beach nourishment projects in 2002 and 2010 (Stevens et al., 2012). Erosion has also occurred immediately south of the inlet, and a dynamic revetment was installed in 2013 to protect the base of South Jetty and reduce erosion impacts (Allan and Gabel, 2016).

Between 2 and 4 Mm^3 of sand-sized sediment is dredged annually to maintain the 10-km long entrance to the federal navigation channel in the mouth of the Columbia River (USACE, 2021) with trailing-suction hopper dredges. The dredged material is predominantly fine sand with particle diameters from 0.15 to 0.25 mm and generally contains less than 3% fine-grained material (<0.063 mm). The dredged material is placed in the Pacific Ocean at one of several designated areas located throughout the region, with between about 10 and 30% of the dredged sediment disposed of at the Deep-Water Site (Fig. 1). Placement at this location effectively removes the sediment from the active littoral system. The remaining sediment that is dredged from the entrance channel is strategically placed in nearshore sites in water depths between approximately 12 and 22 m to enhance the sediment supply to adjacent beaches and provide added protection to the rubble-mound jetty structures at the entrance. The capacity of the nearshore sites is limited to control excess sediment accumulation and wave amplification, minimize impacts to marine resources (e.g., Roegner et al., 2021), and interference with other marine activities (e.g., fishing).

Between 1997 and 2020, approximately 36.5 Mm^3 of sediment dredged from the navigation channel was placed in the Shallow Water Site (~57% of all sediment dredged from the navigation channel) with an average annual placement volume of about 1.5 Mm^3 (USACE, 2021). Annual operational use of the South Jetty Site began in 2014 and a total of about 1.7 Mm^3 was placed in the South Jetty Site between 2014 and 2020. Prior to placement each year and throughout the dredging operations, repeated bathymetry surveys are performed, and specific areas within the sites are identified for placement of sediment such that net deposition does not exceed a target threshold based on a baseline condition. The maximum allowed accumulation for the Shallow Water and South Jetty Sites is 1.5 and 1.2 m, relative to baseline surveys performed in 1997 and 2012, respectively. Waves and currents efficiently disperse sediment placed in the Shallow Water and South Jetty Sites outside of the site boundaries. Less than 2% (about 700,000 m^3) of the 36.5 Mm^3 of sediment placed in the Shallow Water Site has remained within the site based on bathymetric surveys performed between 1997 and 2020. Similarly, bathymetric surveys conducted between 2012 and 2020 suggest that the South Jetty Site has retained about 8% (130,000 m^3) of the 1.7 Mm^3 of sediment placed.

To increase the opportunities for nearshore placement, and thereby more efficiently increase the sediment supply to eroding shorelines north of the inlet, the North Head Site offshore of North Head was selected as a potential placement site in 2018 (Fig. 1). Prior to operational use of the North Head Site beginning in the late summer of 2021, field data were collected that included three separate pilot dredged material placements, extensive bathymetric monitoring, and deployment of oceanographic instruments. In this study, data from the third and largest pilot placement were combined with sediment transport modeling to evaluate the suitability of the site to enhance dispersal, support jetty integrity, and feed adjacent beaches.

3. Methods

3.1. Field data

3.1.1. Berm placement and monitoring

Approximately 216,000 m^3 of sediment dredged from the federal navigation channel by the dredge *Essayons* was placed along the southern portion of the North Head Site between September 15 and September 22, 2020, which required 47 loads to complete. The dredge released the sediment in thin layers across a series of transects oriented from the northwest to southeast in water depths between 12 and 15 m with the intention of creating a broad, low-relief, nearshore berm. Bathymetric surveys were performed immediately prior to (September 9, 2020) and following (September 22, 2020) placement to quantify the initial morphology of the berm and verify the volume of the deposit on the seabed. An additional 5 successive surveys were performed between September 22, 2020, and March 10, 2021, to track the movement and morphologic change of the berm. The bathymetric survey area extended approximately 760 m beyond the initial extent of the berm in all directions to capture the bathymetric change resulting from sediment movement.

Bathymetric surveys were conducted using the survey vessel *Elton* equipped with a Reson SeaBat T50-P multibeam sonar operated at 400 kHz. Depths were computed with sound velocity measurements acquired with either a YSI CastAway CTD or AML X2 Series sound velocity profiler. Positioning was achieved with an Applanix POS-MV Wavemaster II and submersible IMU operating primarily in real-time kinematic mode with differential corrections transmitted via NTRIP from the Oregon Real Time GNSS Network (https://www.oregon.gov/odot/ORGN/Pages/index.aspx). Post-processed positions were applied using Applanix POSPac MMS software when real time communications between the survey vessel and geodetic network failed. Hypack hydrographic software was used for survey data acquisition and post

processing. Elevations relative to mean lower low water (MLLW) were computed using offsets from the National Geodetic Survey Geoid12a geoid model and tidal datum established at Hammond, Oregon. Digital elevation models were produced using processed depth soundings bin averaged onto a regular grid with a horizontal resolution of 5 m.

Metrics to describe the observed change in berm morphology and dispersion rate were calculated in the following manner. Cumulative volume changes within the survey area were computed by differencing successive surveys to the pre-placement survey performed on September 9, 2020. A potential bias of ± 3 cm between surveys was used to illustrate how relatively small vertical offsets between surveys would influence the calculations of berm volume. The extents of the deposit were defined based on vertical changes greater than 3 cm between the pre-placement survey and successive surveys. Within the computed extent of the berm, the area, maximum height, mean height, and volume centroid of the deposit were computed.

3.1.2. Oceanographic observations

Time-series measurements of waves, currents, and water properties were collected at a single moored buoy within the North Head Site (Fig. 1), located just north of the berm survey area. The buoy was deployed approximately one year prior to placement of the dredged material on August 28, 2019, to characterize hydrodynamic processes at the site. The buoy consisted of an AXYS Technologies TRIAXYS wave buoy, downward-looking Nortek Aquadopp 400 kHz ADCP, and three Star ODDI CTD sensors located at approximately 1, 5, and 12 m below the surface. Directional wave data were measured at 4 Hz in burst durations of 20 min every 30 min. Vertical profiles of current velocity were measured from 2.5 m below the surface to the seabed with a vertical resolution of 1 m. Velocity profiles recorded every 30 min were based on measurements collected at 2 Hz intervals for 15 min. Conductivity, temperature, and depth were measured at 5–10 min intervals at each of the three locations within the water column. The buoy was recovered on October 1, 2019, resulting in a 34-day deployment. Meteorological observations were obtained from a second buoy located roughly 1.5 km to the northwest that was deployed by Center for Coastal Margin Observation and Prediction (CMOP; Fig. 1).

3.2. Numerical model

The process-based hydrodynamic and sediment transport model Delft3D (version 4.04.01) was used to simulate the dispersion of sediment from the nearshore berm. Hindcast simulations were performed for two time periods: 1) August 26 – October 2, 2019, during the oceanographic buoy deployment for validation of hydrodynamic parameters, and 2) September 22, 2020–March 10, 2021, coinciding with the observations of berm morphology. The model simulations were used to evaluate model performance, characterize physical processes, and predict the fate of the berm sediment outside of the bathymetric survey area. Previous applications of the Delft3D modeling system to the mouth of the Columbia River from which the present model was adapted (Elias et al., 2012; Stevens et al., 2020) have shown the model capable of simulating complex processes such as interaction of strong tidal currents and highly variable density stratification, waves and wave-current interaction, tidal asymmetry, and related mean flow in the system, and the wetting and drying of large tidal flats and wetlands in the lower estuary. Additional information on the Delft3D modeling system, including testing and validation of the Delft3D Online Morphology system, was reported in Lesser et al. (2004) and Lesser (2009).

3.2.1. Delft3D flow

The long time period and high spatial resolution required for this study necessitated a nested modeling scheme to reduce computational expense. The nested detail model domain consisted of a structured, orthogonal, curvilinear grid that covers an area of 37 km along shore and 33 km cross shore centered on the inlet (Fig. 2). The grid contained 140 by 246 cells with resolution varying between 26 m and 1.2 km. Ten equally spaced vertical sigma layers were used to simulate 3D effects within the model domain. The grid was aligned with coastal engineering structures, including the three primary stone jetties, as well as several training dikes along the north side of the navigation channel. Flow through the structures was limited in the model by using thin dams (no transmission) or dry points. The open boundaries in the detailed model were prescribed as a time-series of Riemann invariants (Verboom and Slob, 1984) and salinity values for each vertical layer derived from an overall model domain (Fig. 2) that extended roughly 150 and 100 km to the north and south of the inlet, respectively.

The bathymetry for the overall, detailed, and wave grids was derived from datasets collected by the U.S. Geological Survey (USGS), NOAA, and USACE between 2004 and 2020 (Stevens et al., 2019; Gelfenbaum et al., 2015; https://www.ncei.noaa.gov/maps/bathymetry/). A previously published digital elevation model of the lower Columbia River (Lower Columbia Estuary Partnership, 2010) was used for the tidal river between the Astoria Bridge and The Beaver Army Terminal, the fluvial

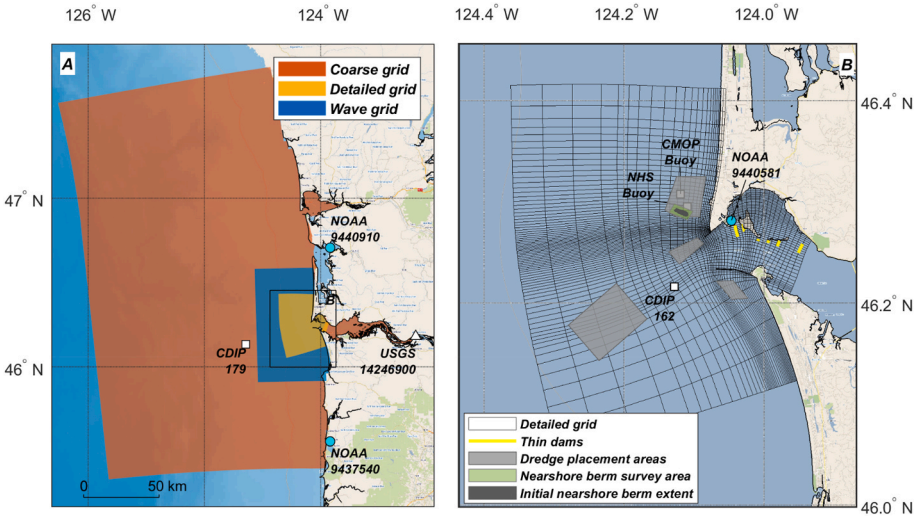

Fig. 2. Maps of Delft3D model application including *A*, extents of Delft3D flow coarse, detailed, and wave domains, and *B*, computational grid of the detailed model (reduced by a factor of 3 for display). The locations of wave buoys, tide gauges, and stream flow measurements used for model boundary conditions are shown in *A*. The locations of oceanographic moorings and tide gauges used for model validation are shown in *B*.

boundary. A regional digital terrain model (Love et al., 2012) was used in areas where more recent datasets were not available. The source bathymetric data were converted to a common reference frame (NAD83) and to the land-based North American Vertical Datum of 1988 (NAVD88), then projected into the Cartesian UTM Zone 10 coordinate system (meters). Deep areas associated with the Astoria submarine canyon were removed from the model bathymetry to improve stability along the oceanic boundaries.

Oceanic boundaries of the overall model were forced using astronomic tidal constituents derived from the TPXO 7.2 global tide model (Egbert and Erofeeva, 2002). A vertical offset of 1.15 m (positive values are up) derived from NOAA VDatum (version 3.2; Xu et al., 2010) was applied at the oceanic boundary to account for the difference between local mean sea level and NAVD88. Water levels in the mouth of the Columbia River and estuary are influenced by coastal processes such as regional upwelling and downwelling events that induce variations at subtidal frequencies and propagate upriver (MacMahan, 2016). These oceanic subtidal variations in sea surface height were imposed at the oceanic open boundary as a time-varying correction to the astronomical tides. The subtidal time-series was derived from observations of water levels at NOAA stations 9440910 (Toke Point, WA), 9437540 (Garibaldi, OR), and 9440581 (Cape Disappointment, WA). Water-level time-series from the three stations were low-pass-filtered using a 66-hr cutoff to remove fluctuations at tidal frequencies. The low-pass-filtered values from the stations were highly correlated, and an average was applied to the oceanic model boundaries.

The landward boundary of the overall model was forced with a time-series of river discharge measured at 30-min intervals at USGS gauge 14246900 (Fig. 2; http://waterdata.usgs.gov/usa/nwis/uv?site_no=14246900; U.S. Geological Survey, 2021). The overall model's oceanic and fluvial boundaries were prescribed constant salinity values of 33 and 0 practical salinity units (psu), respectively. Following Elias et al. (2012), who performed extensive validation of the hydrodynamics in the Columbia River inlet, the effects of temperature variations on circulation were neglected in the present model application.

3.2.2. Wave model

The spectral wave model SWAN (version 41.31) was applied to both overall and detailed models to simulate waves from the continental shelf to the coastline. SWAN was used to simulate the evolution of wave action density using the action balance equation (Booij et al., 1999) on a grid that was slightly larger than the detailed flow model. Wave energy was discretized into 48 frequency bins between 0.03 and 1 Hz and 36 directional bins that covered a 180-degree sector from south to north. The seaward open boundary approximately intersects the location of Coastal Data Information Program (CDIP) buoy 179 at a water depth of 181 m. The 2D, spatially uniform, time-varying energy spectra derived from measurements at CDIP buoy 179 were used to force the wave model. Space- and time-varying wind fields derived from the High Resolution Rapid Refresh (HRRR) atmospheric model (Blaylock et al., 2017) were applied to simulate wind-wave growth within the model domain. Physics in the third-generation mode were based on ST6 formulations described in Rogers et al. (2012). The JONSWAP bottom friction model with a coefficient of 0.038 m^2s^{-3} and default settings for depth induced breaking and triads were included. Convergence criteria were set to 99 percent of cells and a maximum of 30 iterations to obtain full convergence for all wave cases.

The overall and detailed coupled wave and flow models were run with a computational time step of 6 s to fulfill courant stability criteria and ensure stable and accurate results. Two-way coupling between the wave model and flow model involved a nonstationary hydrodynamic calculation in combination with regular stationary wave simulations. SWAN was activated every 30 min during the hydrodynamic simulation, and, using the water levels and depth-averaged currents passed from the flow model, performed a stationary wave simulation. Wave-enhanced bottom stresses in the flow model were applied according to Fredsøe (1984).

3.2.3. Sediment transport model

The online morphology addition to Delft3D was used to simulate sediment transports in the detailed domain at each computational time step (Lesser et al., 2004). The van Rijn (1993) formulation, which separates the sediment transport into suspended and bed load components, was used to model the movement of non-cohesive sand fractions. Default parameters in the sediment transport formula were retained apart from the wave-related suspended (SusW)- and bed load (BedW)-transport coefficients which varied between 0.1 and 0.4 during model calibration. These two coefficients influence the magnitude of bed load transport (BedW) and suspended transport (SusW) in the direction of wave propagation due to wave asymmetry. Previous studies have noted that default values of 1 for these two coefficients leads to overestimation of onshore sediment transport (Grunnet et al., 2004), and recent sediment transport model applications using Delft3D often reduce these coefficients by up to 90% (e.g., Nienhuis et al., 2016; Hopkins et al., 2018). See Deltares (2018) for a full description of the implementation of the van Rijn (1993) transport formula.

Separate sediment fractions with the same properties were used to represent native and berm sediment. The inclusion of two separate sediment fractions in the model simulations facilitated the tracking of the berm sediment throughout the model domain. Each simulation utilized a single, uniform grain size and the grain sizes of native and berm sediment fractions varied between 0.15- and 0.25-mm during model calibration. Bed stratigraphy was activated in the model, which allows for sediment deposited on the bed to be vertically incorporated into the sediment profile, and a total thickness of 20 m of sediment was made available for all model simulations. The thicknesses of the transport- and under-layers of the bed stratigraphy element varied between 5 and 40 cm during model calibration. The transport layer represents the top layer of the seabed and the composition of the transport layer changes as a result of predicted erosion and deposition during the simulation. The transport layer exchanges sediment with the first under layer directly below (also referred to as the exchange layer) while farther down in the bed, the under layers are vertically fixed. See van der Wegen et al. (2011) and Huisman et al. (2018) for more detailed descriptions of the bed stratigraphy module implemented in Delft3D. The initial spatial distributions of berm and native sediment fractions were determined based on observed nearshore berm extent and thickness interpolated onto the computational grid.

Bed level updating during the simulations was deactivated (i.e., morphostatic conditions) to isolate the sediment transport patterns that result from the interaction of hydrodynamic processes with the observed morphologic features. This morphostatic approach has been adopted elsewhere when predicted morphologic changes are small relative to hydrodynamic processes (e.g., Grasso et al., 2021; Pearson et al., 2020) over the time frame considered. We argue this assumption is valid given the relatively small extent and low relief of the berm and modest changes in berm geometry over the study period (see Section 4.2). The total mass of each sediment fraction was computed for each grid cell and vertical layer in the bed throughout the model simulations. Convergences and divergences in sediment transport resulting in changes in the mass of berm sediment at each grid cell were used to quantify potential erosion, deposition, and berm thickness assuming a dry sediment density of 1600 kg/m^3. Metrics describing changes in the simulated berm morphology were computed using the same methodology applied to the observations described in section 3.1.1.

4. Results

4.1. Hydrodynamic model validation

Previous applications of the Delft3D model for the mouth of the Columbia River have been validated against field data (waves, currents,

water column properties) collected within the Columbia River inlet during both high and low river discharge conditions (Elias et al., 2012; Stevens et al., 2020). Here, we present additional comparisons of model predictions to observations collected outside the inlet to evaluate the accuracy of the modeled hydrodynamics within the North Head Site and the new source of meteorological forcing. Observations of bulk wave parameters and near-bed current velocities at approximately 2.2 m above the bed collected at the North Head Site buoy were compared against model predictions during low energy conditions for the interval of August 28 to October 1, 2019. Additional comparisons of wind velocity and water levels during the same time interval were derived from observations at a nearby buoy deployed by CMOP and at the NOAA tide station 9440581, respectively. Metrics describing comparisons between modeled and measured parameters were computed following Willmott (1982). Qualitative and quantitative comparisons between modeled and measured water levels, wind velocities, and bulk wave parameters show good agreement (Fig. 3; Table 1). However, model performance for the near-bottom currents was less accurate, with a skill score of 0.48 and 0.56, for eastward and northward velocity components, respectively. Section 5.1.1 provides further details on model performance and consideration of the relative importance of the measured hydrodynamic parameters on sediment transport and morphology predictions.

4.2. Sediment transport and berm morphology

Immediately following the placement of sediment by the hopper dredge within the North Head Site, multibeam bathymetric surveys confirmed the creation of a distinct morphologic feature on the seabed that was approximately 1.5 km long and 500 m wide with a maximum height of 0.7 m (Fig. 4) and a volume of 204,000 m^3. Successive bathymetric surveys performed throughout the fall and winter quantified the movement and dispersal of the berm. Minimal movement was observed between September 22 and October 26 coinciding with a period of low mean and maximum wave heights at nearby CDIP wave buoy 162 (1.9 and 4.4 m, respectively). Wave energy increased significantly between October 26 and December 2 (mean and max wave heights were 2.5 and 6.8 m, respectively), and the berm moved onshore and thinned though the areal extent decreased. A greater change in berm morphology was observed between December 2 and December 29 when the mound spread primarily in the onshore direction and the measurable extent of the berm increased and extended to edge of the onshore boundary of the survey area (Fig. 4E). The total volume of sediment in the deposit decreased suggesting dispersal of sediment outside of the observed survey area. The berm continued to spread, thin, and move onshore for the remainder of the observation interval. At the time of the final bathymetric survey on March 10, 2021, the observed volume

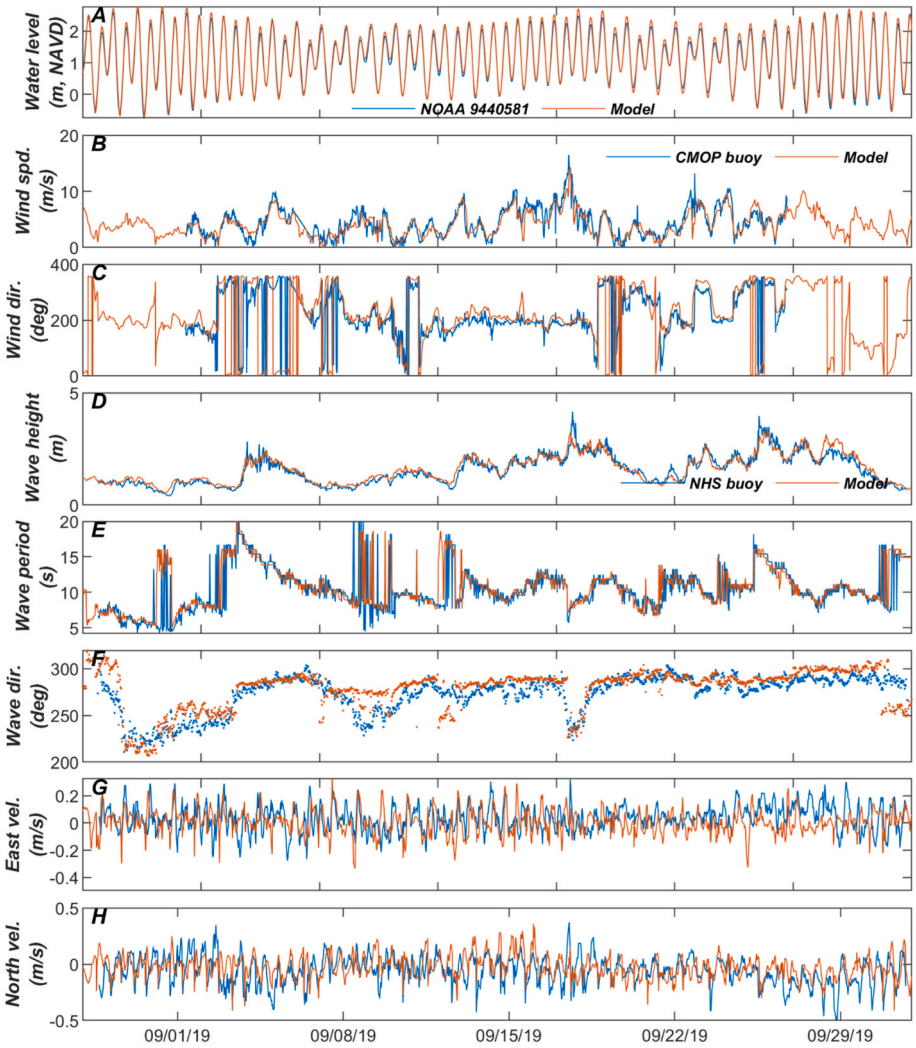

Fig. 3. Time series comparisons of measured and modeled *A*, water levels measured at NOAA Site 9440581, *B–C*, wind speed and direction measured at CMOP buoy, *D-F*, wave parameters measured at NHS buoy, and *G-H*, near-bottom current speeds measured at NHS buoy. See Fig. 2 for locations of measurement sites used for hydrodynamic model validation.

Table 1
Metrics describing comparisons between modeled and measured hydrodynamic parameters. RMSE, RMSU, and RMSA represent the root-mean-square (RMS) error, bias-corrected RMS error, and systematic RMS error, respectively.

Parameter	Site	Obs. Avg.	Model Avg.	RMSE	RMSU	RMSA	Skill
Water level (m)	NOAA 9440581	1.16	1.21	0.11	0.09	0.07	0.99
Wind Speed (m/s)	CMOP Buoy	4.11	4.43	1.36	1.32	0.32	0.91
Wave Height (m)	NHS Buoy	1.61	1.55	0.22	0.21	0.06	0.97
Wave Period (s)	NHS Buoy	10.76	10.38	2.21	1.97	1.00	0.84
East Velocity (m/s)	NHS Buoy	0.01	0.04	0.12	0.09	0.08	0.48
North Velocity (m/s)	NHS Buoy	−0.02	−0.06	0.14	0.12	0.07	0.56

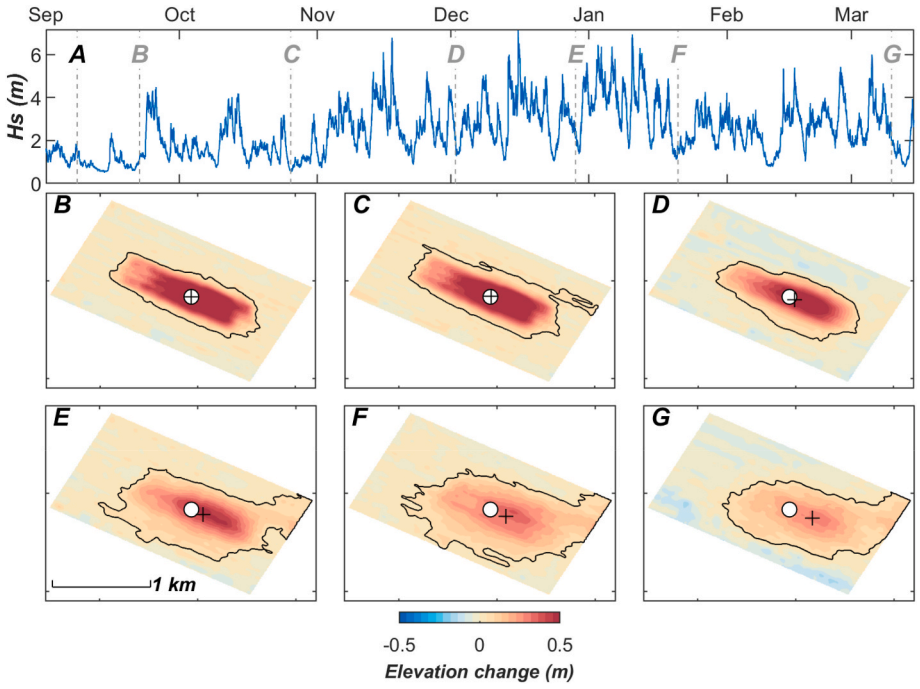

Fig. 4. Observations of wave conditions and berm morphology between September 22, 2020, and March 10, 2021, showing *A*, time series of significant wave height measured at CDIP Site 162, and *B-G*, berm height for each successive survey. The extent (black outlines, defined using a 3 cm elevation change threshold), initial centroid (circles), and time varying centroid (plus signs) of the berm are shown in *B-G*. See text for details on quantification of berm metrics and Fig. 2 for the location of CDIP buoy 162. Gray lines in *A* denote the timing of bathymetric surveys. Spatial extent of the survey in *B-G* is shown in Fig. 1.

within the berm had decreased by about 40% to127,000 m^3, the measurable extent of the berm increased although the full extent was likely outside of the survey area, the maximum height lowered by almost 60% to 0.3 m, and the center of the deposit moved onshore over 200 m. In section 4.3, we use these observations to evaluate predictions of sediment transport and berm morphology from the hydrodynamic and sediment transport model.

4.3. Sensitivity to model parameters

Hindcast simulations over the time interval of the repeat bathymetry surveys (Sept. 22, 2020, to March 10, 2021) were performed with a variety of transport formula coefficients, bed schematization parameters, and grain sizes to better understand the effects of these parameters on sediment transport fluxes (Fig. 5; Table 2). Comparisons between modeled and observed near-field berm morphology metrics were quantified for each simulation to determine the ability of the model to reproduce the observed change in berm morphology over time and constrain uncertainty in input parameters. Each run required approximately 13 days to complete on a PC equipped with a 3.9 GHz (base speed) processor (AMD Ryzen 3800X) running on 8 cores with DDR4 memory running at 3600 MHz to simulate the full time period of berm morphology observations. Therefore, only a limited number of sensitivity computations were performed due to computational expense.

Variations in the thicknesses of the transport- and under-layers (Fig. 5A–C) and values of the wave related transport formula coefficients (Fig. 5D–F) had similar effects on sediment fluxes and dispersal of berm sediment from its placement location. Model simulations with thinner bed layers and larger wave-related transport coefficients resulted in larger onshore fluxes and vice-versa. Smaller onshore fluxes associated with thicker bed layers and smaller wave related transport coefficients resulted in less sediment reaching the surf zone to be transported alongshore by wave driven currents. The alongshore component of sediment fluxes was sensitive to variations in grain size (Fig. 5G–I). Simulations with a grain diameter of 0.15 mm resulted in little net onshore transport from the berm location while onshore sediment fluxes were dominant with larger grain sizes.

The variability in sediment fluxes based on different bed layer thicknesses, transport formula coefficients, and grain sizes described above affected predicted berm morphology over time. The impacts on berm morphology metrics related to variations in wave related transport parameters and bed layer thickness were larger than those associated with grain size (Fig. 6). The volume of sediment within the berm was most sensitive to variations in transport formula coefficients (Fig. 6A). At the end of the monitoring period, the predicted berm volume varied by 44% between 70,000 and 160,000 m^3 for simulations with high and low transport coefficients, respectively. Despite this sensitivity, all predicted berm volumes fell within the range of volumes derived from repeated multibeam survey observations based on a potential bias of ±3 cm at the end of the study.

The areal extent, berm height, and movement of the berm centroid were most sensitive to variations in the thicknesses of the transport- and under-layers used to schematize bed stratigraphy (Fig. 6B–D). In all simulations, the areal extent of the berm initially increased and

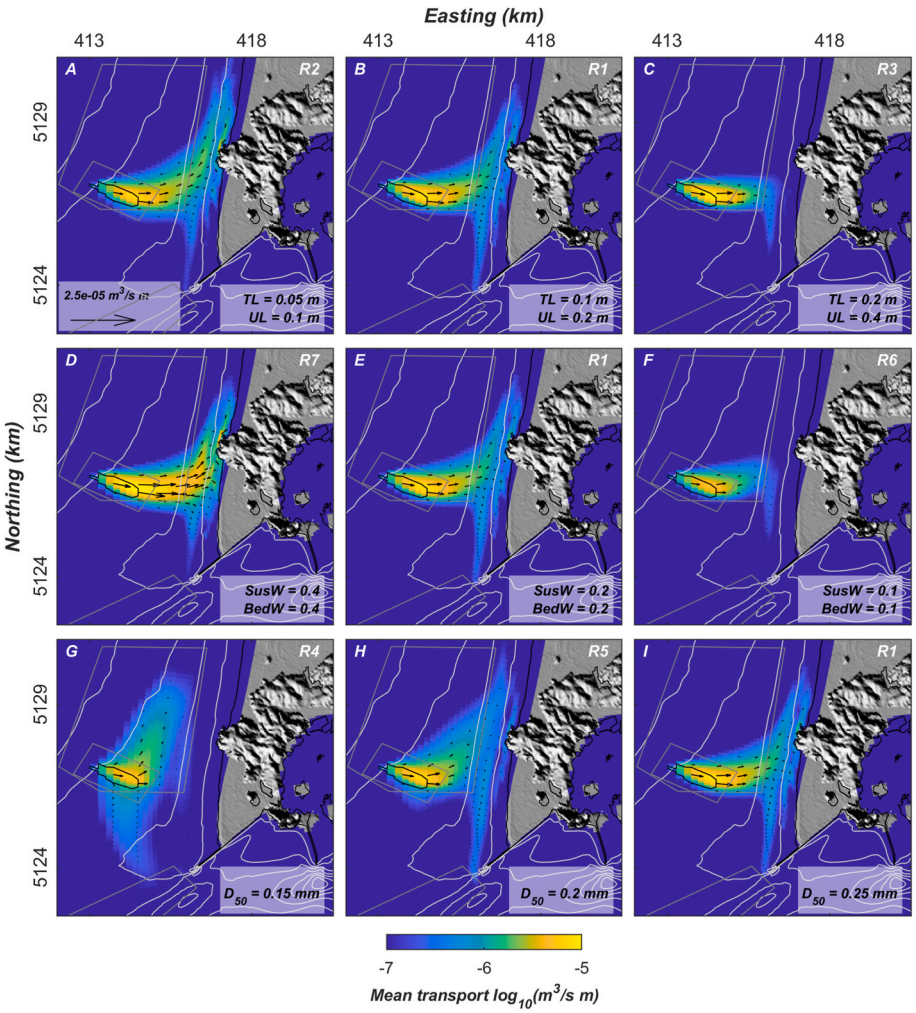

Fig. 5. Mean transport of berm sediment during 169-day hindcast between September 22, 2020, and March 10, 2021, showing sensitivity to *A-C*, thicknesses of transport layers (TL) and under layers (UL), *D-F*, sediment transport coefficients (SusW and BedW), *G-I*, median grain diameter (D_{50}). See Table 2 for parameters used in each simulation.

Table 2
Model features and parameter settings of sensitivity runs.

Run ID	Wave-related transport coefficients (SusW and BedW)	Transport-layer thickness (m)	Under-layer thickness (m)	Sediment grain size (mm)
R1	0.2	0.10	0.20	0.25
R2	0.2	0.05	0.10	0.25
R3	0.2	0.20	0.40	0.25
R4	0.2	0.10	0.20	0.15
R5	0.2	0.10	0.20	0.20
R6	0.1	0.10	0.20	0.25
R7	0.4	0.10	0.20	0.25

subsequently decreased over time (Fig. 6B). Thinner bed layering resulted in an earlier and larger magnitude decrease in berm extent compared to simulations with thicker bed layering. The observed areal extent of the berm fell within the predicted range of simulated values at the end of the study.

All simulations predicted the berm to decrease in height over time regardless of input parameters (Fig. 6C). Thicker transport- and under-layers resulted in more thinning of the berm over time compared to simulations with thinner bed layers. Simulations with thin bed layers overpredicted the berm height compared to observations at the end of the simulation, while medium and larger bed layers more accurately reproduced the final thickness of the berm.

Thicker bed layers resulted in more onshore movement of the centroid of the berm deposit within the near field and vice versa (Fig. 6D). The simulation with larger bed layers overestimated onshore movement and thinner bed layers resulted in less onshore movement of the deposit centroid compared to observations. More onshore displacement of the berm within the nearfield survey area (Fig. 6D) for simulations with larger bed layers contrasts with overall reduced onshore sediment fluxes throughout the model domain (Fig. 5C). None of the simulations were able to reproduce the magnitude of the south-directed, alongshore movement of the berm deposit, though the centroid of the deposit did move to the south slightly in simulations with larger bed layers, while the berm centroid in the simulation with small bed layers moved to the north.

4.4. Ranking of model performance

For each berm morphology metric and simulation, the performance of the model was quantified using the discrepancy between modeled and measured value as a percentage at the end of the simulation (Table 3). The final simulated morphology was favored over time-dependent comparisons to better simulate dispersion of sediment time scales most relevant to management practices (e.g., annual dredging). No single simulation best represented all measured berm morphology metrics at the end of the hindcast. Rather, the simulations were ranked by summing the fractional errors over all morphology metrics. The two

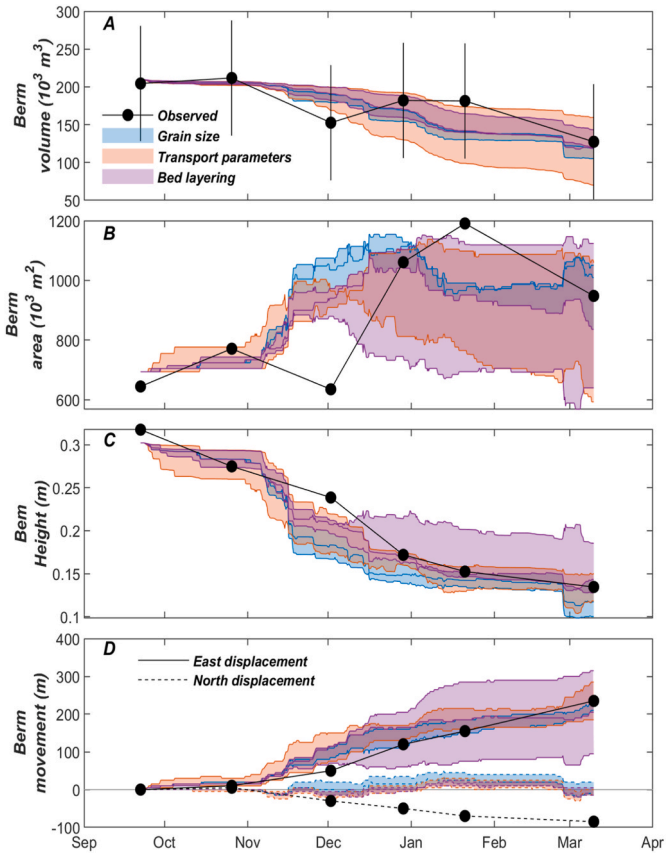

Fig. 6. Comparisons between measured (black dots) and simulated berm morphology metrics (colored lines) including *A*, berm volume, *B*, berm area, *C*, mean berm height, and *D*, movement of the berm centroid over time. For each morphology metric, model results are shown for simulations with a variety of grain sizes, transport formula coefficients, and bed layer thicknesses. See Table 2 for the parameters used in the model simulations. Error bars in A represent potential bias between initial and successive surveys of ±3 cm.

simulations that performed best overall (R1 and R5) utilized the same transport coefficients and bed layer schematization but differed in the grain size used. These two simulations performed similarly in terms of cumulative total error and were both used to evaluate the dispersion and fate of berm sediment outside of the measurement area and provide a range of plausible outcomes based on the available data. Qualitative assessment of the best-performing model hindcast showed good agreement between simulated and observed berm morphology (Fig. 7).

4.5. Fate of nourishment

Model simulations universally predicted that sediment dispersed outside the survey area continued to move primarily onshore, was incorporated into the littoral zone, and was transported north and south following the time-variable wave-driven currents (Fig. 5). Sediment transport, however, primarily occurred during episodic intervals that coincided with large wave events between November 2020 and February 2021 (Fig. 8). High near-bed currents transported large quantities of sediment in suspension during the largest transport events, while more moderate events resulted in roughly equal suspended and bed load transports. Transport patterns for 0.2 and 0.25 mm (Fig. 5H–I) sediment were very similar except that finer particles were dispersed more to the north while coarser sediment was transported more directly onshore before intersecting the surf zone.

Of the initial 204,000 m^3 initially detected in the berm, the best (or the optimal) model simulations (R1, R5) suggested that approximately 90,000–91,000 m^3 was dispersed from its initial placement location over the study time period (Sept. 22, 2020, to March 10, 2021). The berm was relatively stable between September 22 and October 26, 2020 (Fig. 9A–B), coinciding with a time period of low wave energy. Initial widespread dispersal of berm sediment was predicted between October and December 2, 2020 (Fig. 9C), and was directed onshore as a series of larger wave events from the northwest impacted the area. Waves approaching the berm shifted to a more westerly direction between December 2, 2020, and January 21, 2021. During this time, sediment from the berm was transported onshore and to the north, largely bypassing Benson Beach, and accumulating in shallow water north of North Head (Fig. 9E). Significant quantities of sediment from the berm began depositing within the nearshore areas off Benson Beach after a series of wave events from the northwest between January 21 and March 10, 2021. The northwesterly wave events during this time period transported sediment from the berm onshore directly toward Benson Beach. In addition, sediment that initially deposited north of North Head was transported south by wave driven currents and accumulated along Benson Beach.

A sediment budget was developed using the simulations that performed best during model validation (R1, R5). These two simulations had similar error metrics (Table 3) and similar amounts of sediment was dispersed away from the initial extent of the berm (Fig. 10). However, the fate of sediment for these two simulations differed in the amount and location of sediment that accumulated along the coastline. A larger percentage of sediment placed in the berm was transported to Benson Beach for simulation R1 with larger sediment size. By the end of the model simulation, between 9 and 17% of the initial volume of sediment released at the placement site was predicted to accumulate along the shoreface of Benson Beach. Between 32 and 45% of the berm sediment had dispersed outside of the initial footprint and accumulated in between the placement area and Benson Beach or was transported to the north of North Head along the Long Beach Peninsula. The remaining 47–51% of the berm sediment remained within the initial extent of the berm 169 days following placement.

4.6. Comparison of nearshore placement sites

Model scenarios were carried out to compare dispersion rates, transport pathways, and the fate of sediment from hypothetical berms placed in other locations used for operational dredged material placement. Hypothetical berms with the same morphology were placed in the Shallow Water and South Jetty Sites that are currently used

Table 3
Fractional (simulated/observed) errors in berm morphology metrics at the end of the monitoring period. Cumulative errors reflect the sum of errors for individual metrics and were used to rank the performance of the various simulations.

Run ID.	Volume	Area	Mean height	East displacement	North displacement	Cum. Error	Rank
R1	−0.06	−0.12	0.07	−0.13	−0.82	1.19	2
R2	−0.07	−0.32	0.38	−0.60	−1.06	2.43	7
R3	0.13	0.19	−0.05	0.34	−0.82	1.53	3
R4	−0.18	0.11	−0.26	−0.11	−1.24	1.88	5
R5	−0.07	0.06	−0.13	−0.02	−0.88	1.17	1
R6	0.25	0.12	0.12	−0.21	−1.00	1.70	4
R7	−0.45	−0.37	−0.12	0.21	−0.82	1.98	6

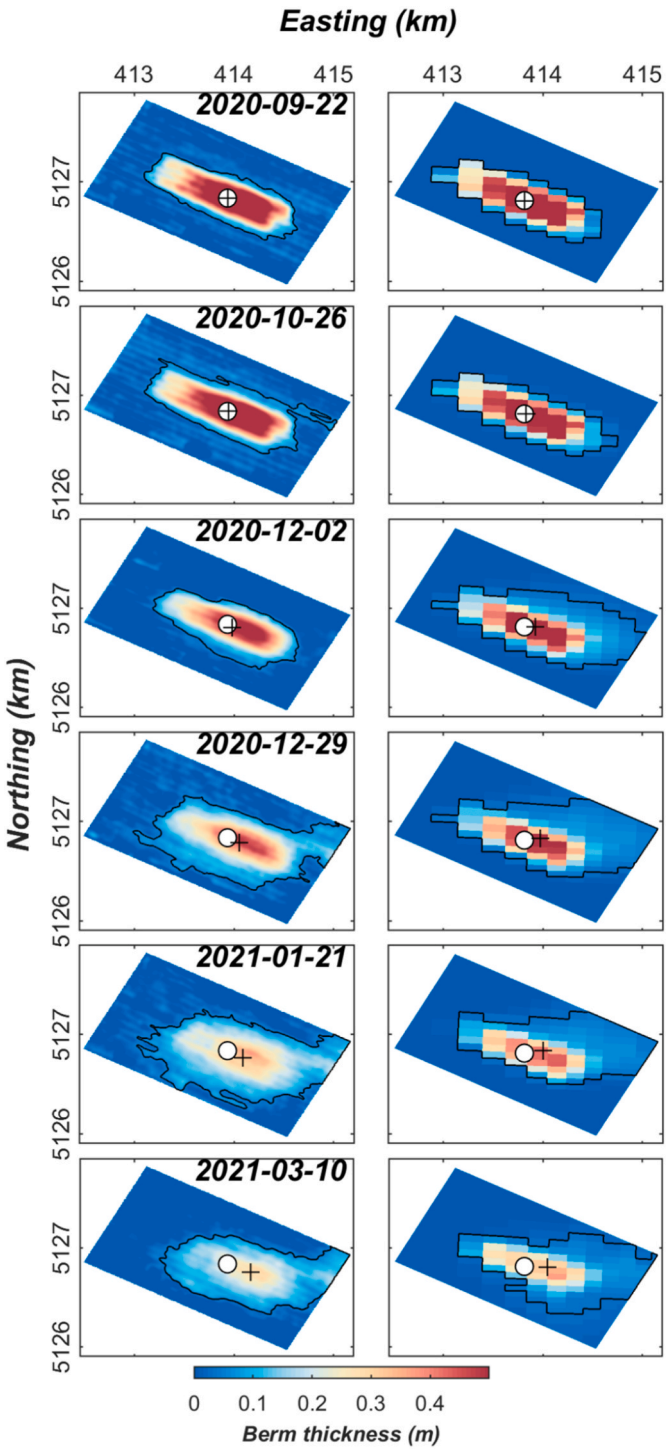

Fig. 7. Observed (left panels) and modeled (right panels) berm morphology over time. Model results derived from simulation with best overall performance (R5, Table 3). Additional caption details as in Fig. 4.

operationally for annual thin-layer placements, as well as the northern portion of the North Head Site to compare with results from the actual berm placed in the southern portion of North Head Site (Fig. 11A). The orientation of the hypothetical berms was rotated to better fit within the established site boundaries. The models were run separately to avoid interactions between sediment fractions from different berms over the same time period and used the same set of forcing conditions, bed layering, and transport formula coefficients to enable direct comparisons of sediment dispersion and fate.

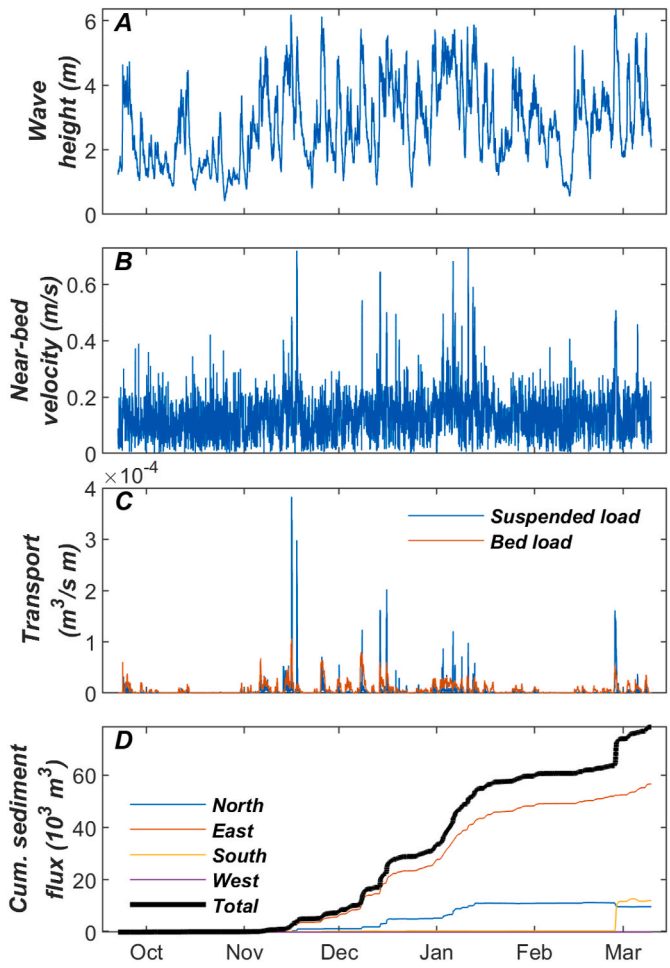

Fig. 8. Time series of, *A*, significant wave height, B, near-bed current velocity magnitude, C, instantaneous bed- and suspended load transports, and *C*, cumulative sediment flux through cross sections. Positive cumulative sediment fluxes represent transport out of the initial placement zone. The locations of the cross sections (red lines) and location of time series output (white circle) are provided in Fig. 9A.

Hypothetical berms placed at northern portion of the North Head Site (NHS N) and South Jetty Site (SJS) were dispersed primarily in the onshore direction at similar rates to the actual berm observed in the southern portion of the North Head Site (NHS S; Fig. 11B). The percentage of berm sediment remaining within the initial extent of the berm at the end of the simulations were almost identical (49–51%) for these three hypothetical placement sites (Fig. 11C). Likewise, hypothetical berms placed at the northern North Head Site and South Jetty Site thinned at similar rates to southern North Head Site with the mean height of the berm only varying between 14 and 16 cm at the end of the simulation (Fig. 11D).

Compared to other berm locations, stark differences in the dispersion rates and transport pathways were predicted for the hypothetical berm placed at the Shallow Water Site (SWS) near the river inlet (Fig. 11). Most of the berm sediment at this site rapidly dispersed away from the initial placement location and in the offshore direction. A smaller amount of sediment was transported onshore and accumulated in the vicinity of the North Jetty (Fig. 11B). Almost 70% of sediment placed within the berm in the Shallow Water Site had dispersed during the first 45 days (Fig. 11C). During this same interval of time, berms placed at other sites were stable. By the end of the simulation, only 1% of sediment placed within the Shallow Water Site remained within the initial extent of the berm and the mean thickness had reduced to less than 1 cm (Fig. 11D).

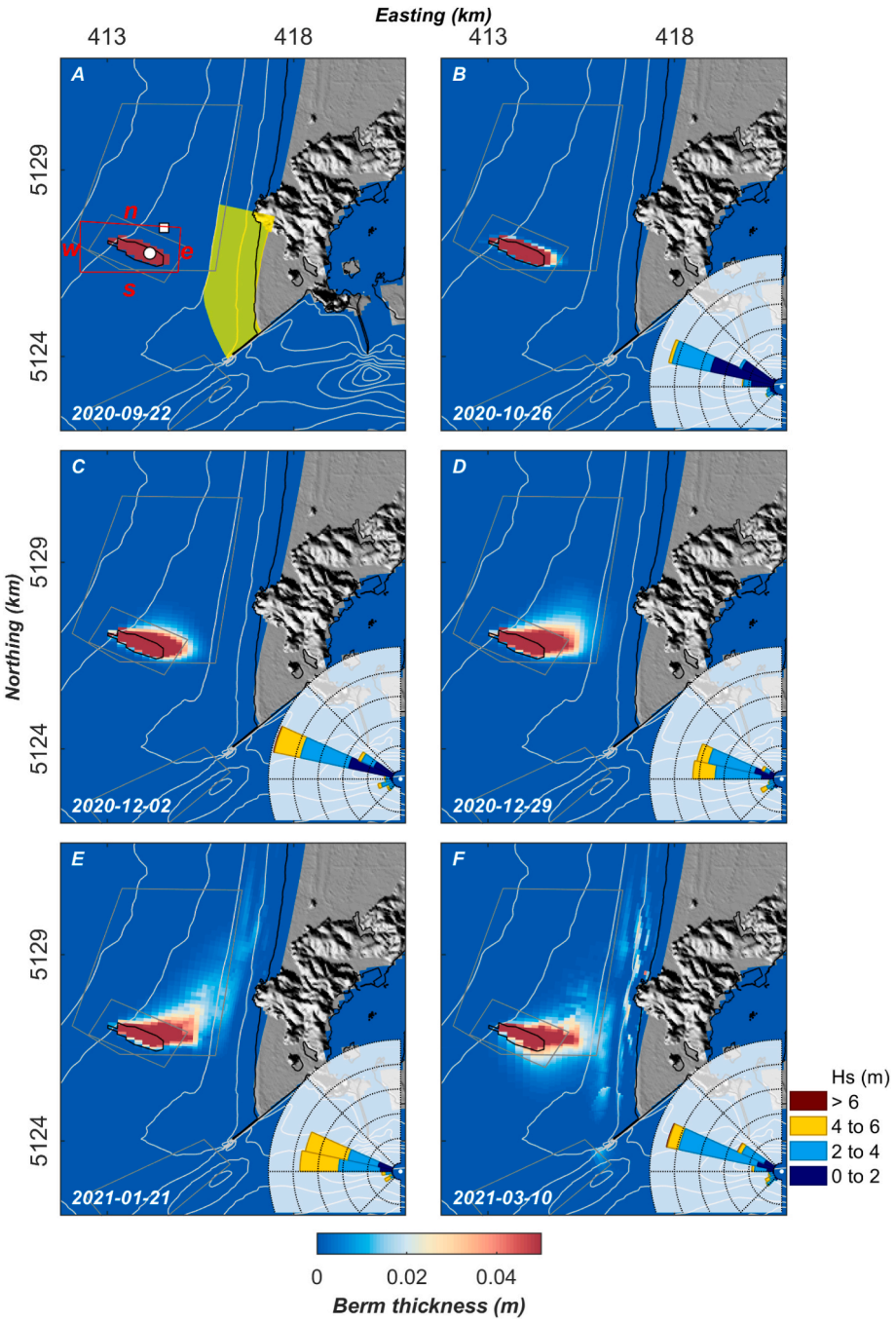

Fig. 9. Maps showing simulated accumulation of berm sediment for model run R5 at the time of each bathymetric survey. Insets in *B–F* show distributions of wave heights and directions between successive surveys. The locations of Benson Beach (yellow polygon), cross sections (n,e,s,w; red lines) used for cumulative sediment fluxes, wave model output (white square), and time series parameters shown in Fig. 8 (white circle) are provided in A.

All the hypothetical berm locations, except for the South Jetty Site, enhanced the sediment supply to Benson Beach (Fig. 11E). Sediment accumulation within the Benson Beach polygon during the hindcast was highest for the berm placed at the southern North Head Site. The total volume of sediment in the Benson Beach polygon from berms initially placed in the northern North Head Site and Shallow Water Site was 25 and 41% that of the southern North Head Site, respectively. The majority of sediment accumulation along Benson Beach from berms placed on the southern North Head Site and Shallow Water Site occurred between December 2020 and February 2021. During this time very little sediment from northern North Head Site accumulated in Benson Beach and most of the total sediment from northern North Head Site occurred during a short time span that coincided with strong wave events from the northwest.

5. Discussion

Strategic placement of dredged sediment has been used to restore and enhance nearshore sediment budgets in a variety of coastal environments from high energy, sandy coastlines (Mendes et al., 2021) to low energy, muddy embayments (Baptist et al., 2019) throughout the world. The designs and techniques used to observe and evaluate strategic placement projects vary widely based on site characteristics as well as operational and budget constraints. Herein, we describe

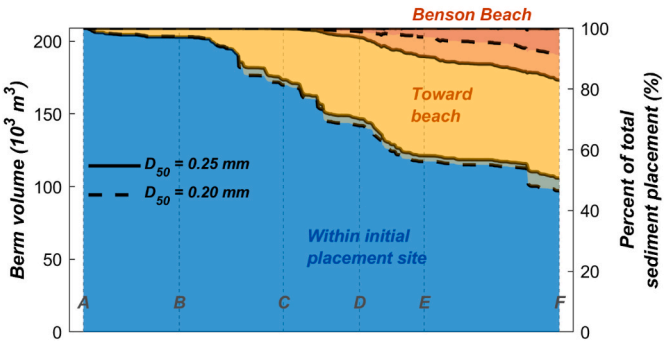

Fig. 10. Time series of sediment dispersion from berm and accumulation in Benson Beach polygon and elsewhere in model domain. Results are shown for two otherwise identical simulations with characteristic median sediment grain diameters (D_{50}) of 0.25 mm (simulation R1) and 0.2 mm (simulation R5). Location of Benson Beach polygon is provided in Fig. 9A and gray lines correspond to times of panels (A–F) shown in Fig. 9. Percent of initial berm volume in each region at end of simulation provided at right.

implementation, monitoring, and analysis of a strategic nearshore placement of dredged sediment that created a broad, low-relief berm in a region with an extreme wave climate (Ahn et al., 2022). A transferable modeling methodology was developed that allowed for the quantification of sediment transport rates and identification of the dominant processes responsible for the dispersal of berm sediment following placement. The berm design, monitoring and modeling framework, and improved understanding of coastal processes discussed below can be used to inform implementation of strategic nearshore placements and regional sediment management in complex, high-energy coastal environments elsewhere.

5.1. Model performance

5.1.1. Hydrodynamics

Model predictions accurately characterized hydrodynamic parameters including water levels, wind speed and direction, and bulk wave statistics for the location of the North Head Site buoy deployed in 2019 (Table 1; Fig. 3). The model performance for these parameters is similar to previous applications of the present Deflt3D model setup (Elias et al., 2012; Stevens et al., 2020) and other models applied for this region including SELFE (Karna et al., 2015) and ROMS (Akan et al., 2017). However, the near-bed currents observed at the buoy location were poorly characterized using the present model setup. Unlike previous studies, where observations were located within the inlet, tidal forcing at the location of the North Head Site buoy, which was used for this comparison, was weak. Currents at this location are necessarily more influenced by other factors including baroclinic circulation, wind and wave processes, and basin-scale coastal currents not captured by our

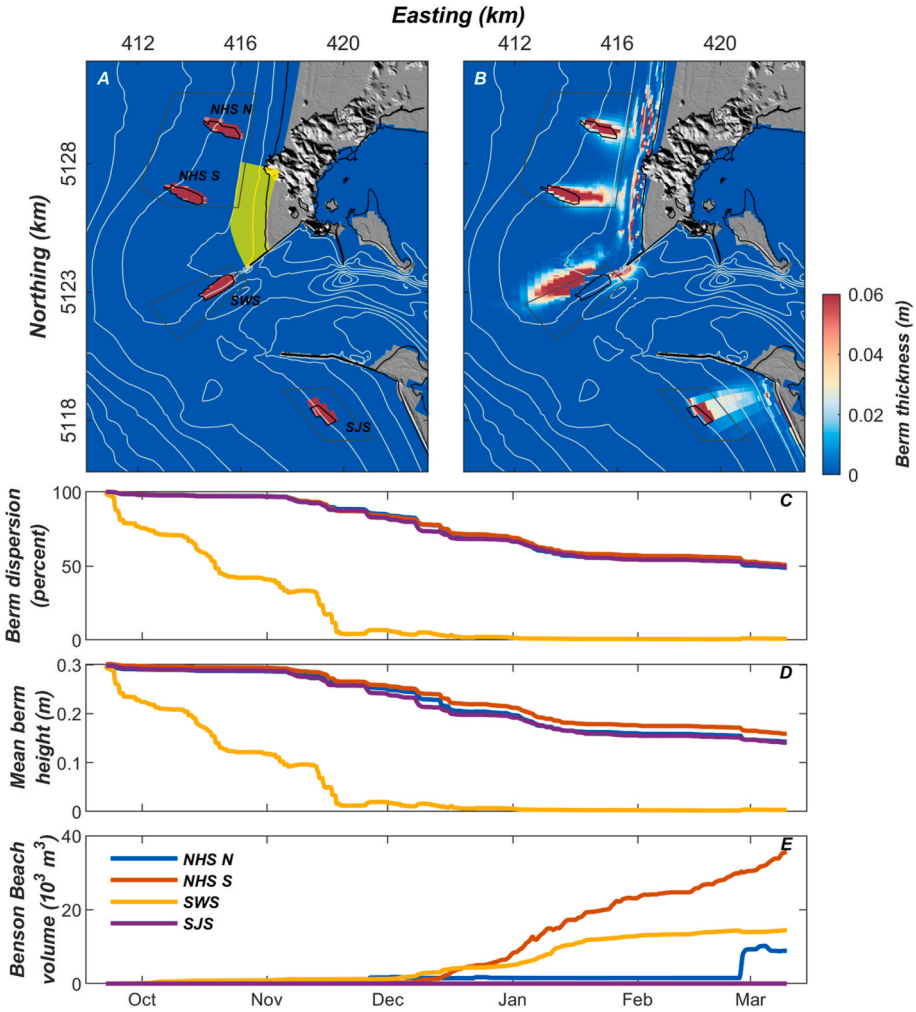

Fig. 11. Results from scenarios with alternate berm placements showing *A*, initial berm placements, *B*, sediment accumulation at the end of 169-day hindcast simulation, *C*, dispersion of berm sediment outside of initial extent, *D*, mean height of berm, and *E*, volume of sediment accumulation within Benson Beach polygon. Locations of initial berm extents (black lines), dredge placement site boundaries (gray polygons), and Benson Beach (yellow polygon) are shown in *A*.

model. Wind and wave effects are well represented in the present model application (Fig. 3), and we suggest the discrepancy between modeled and measured near-bed currents resulted from simplified boundary conditions applied along the oceanic boundaries that did not include variations in density or large-scale coastal circulation. Model performance may be improved by including more realistic forcing on the oceanic boundaries, for example by nesting the model in a regional circulation model such as HYCOM (https://hycom.org). The weak near-bed currents collected at the North Head Site during relatively low wave energy conditions are not often (95th percentile of observed current speeds was 0.31 m/s) capable of transporting sand-sized sediment (van Rijn, 1993a). In addition, the east and north components of mean near-bed currents are roughly symmetrical (Fig. 3), while transport of sediment from the berm is primarily onshore (Figs. 4–5), suggesting wave processes related to asymmetric bottom orbital velocities are primarily responsible for onshore dispersion of sediment from the berm in the direction of wave propagation. We therefore moved forward with the present model application owing to the accurate predictions of wave parameters and berm morphology metrics discussed in section 5.1.2 below.

5.1.2. Sediment transport

The placement of 216,000 m^3 of dredged sediment north of the mouth of the Columbia River in water depths between 12 and 15 m within an area of about 640,000 m^2 created a distinct morphologic feature that was large enough to track with repeated multibeam bathymetric surveys over approximately 6 months (Fig. 4). The measurable volume of the berm immediately following placement was 204,000 m^3, or 94% of the total volume placed. The size, location, and moderate stability of the berm allowed for quantification of metrics describing the berm morphology including total volume within the survey area, area of berm extent, berm height, and displacement of the berm centroid using the bathymetric surveys (Fig. 6). Quantitative comparisons of modeled and measured berm morphology metrics were used to test the sensitivity of key model input parameters to morphologic predictions and evaluate model performance. Whereas other commonly used metrics to quantify error in coastal morphology models such as the Brier skill score (e.g., Sutherland et al., 2004) can favor featureless predictions (Bosboom and Reniers, 2014), this simple methodology ensured that simulations that better represented the large-scale morphologic features of the simulated berm were used (Fig. 7). In addition, the use of multiple metrics describing the berm morphology and dispersion maximized opportunities for model assessment rather than collapsing the comparison into a single metric.

The model was largely able to reproduce the observed change in berm morphology, including the timing and magnitude of volume loss within the survey area, spreading, thinning, and onshore movement of the berm centroid. The mean error, measured as the percent difference between modeled and measured volume, area, thickness, and onshore displacement at the end of the simulation was between 7 and 10 percent in the two best performing simulations (R1 and R5, Table 3). Both model simulations and measured berm morphology suggest the direction of transport following placement of the berm was onshore (Figs. 4–9). Model simulations suggest that the onshore dispersal of sediment from the berm is driven primarily by wave processes, as no transport of berm sediment was predicted during quiescent wave conditions (Fig. 8). The dominant cross-shore exchange of sediment following strategic nearshore placements has been observed elsewhere and wave asymmetry effects have been identified as the process responsible for this onshore movement (Huisman et al., 2019). However, the model was not able to reproduce the measurable southerly (alongshore) displacement of the berm centroid regardless of the settings applied. This discrepancy may be resolved in future model applications with additional sensitivity tests, application of other transport predictors, or inclusion of large-scale circulation along oceanic boundaries to improve the simulated hydrodynamics.

5.2. Model sensitivity and uncertainty

Sediment transport models require a variety of input parameters that can be poorly constrained. Field data are therefore essential to calibrate and reduce uncertainty in model predictions. We identified three input parameters to perform sensitivity analyses and test model predictions of sediment transport: grain size, wave related suspended (SusW) and bed load (BedW) transport parameters that control the magnitude and direction of transports in the van Rijn (1993) sediment transport formula in the direction of wave propagation due to wave asymmetry, and the thicknesses of the transport- and under-layers used to schematize bed stratigraphy (Table 2). Sensitivities to these parameters over the range of values applied varied for each of the predicted berm morphology metrics (Fig. 5). Careful consideration of these model inputs must therefore be taken to accurately simulate transport of sand-sized sediment in energetic, open-coast settings.

The areal extent, mean thickness, and displacement of the berm centroid were most sensitive to the thickness of the transport- and under-layers (Fig. 6B–D). The sensitivity of the berm morphology predictions to the thickness of the transport- and underlayers arises from the modeling approach that utilized two sediment fractions - one for the berm sediment, the other for the native sediment - which had identical physical characteristics, to track dispersion and potential morphology change of the berm. The inclusion of bed stratigraphy is necessary to facilitate and control the rate of mixing between native and berm sediment. Since sediments are assumed to be well-mixed within the bed layers, the rate of changes in composition in the bed, and thus rates of dispersion, are controlled by the thicknesses of the transport- and underlayers. Model applications using multiple sediment fractions to track sediment from a particular location that ignore mixing processes by not making native sediment available everywhere or those that overestimate mixing by using a single, thick, well-mixed layer will lead to erroneously high and low rates of tracer dispersion, respectively. In the present study, good agreement between model predictions and observed morphology of the berm within the survey area was achieved using thicknesses of 0.1 and 0.2 m for the transport layer and under layers, respectively (Figs. 6 and 7; Table 3). However, the rate of dispersion of berm sediment outside of the observed bathymetric survey area is unknown. Physical tracer studies that track dispersion rates of sediment over larger spatial scales (e.g., Li et al., 2019; Pearson et al., 2021) could supplement available information and inform appropriate bed schematization to improve predictions of berm dispersal and fate.

The volume of sediment dispersion out of the survey area was controlled primarily with the transport parameters SusW and BedW (Fig. 6A). We note that the range of values of BedW and SusW applied (0.1–0.4) were much lower than the default (1.0). Default values of BedW and SusW resulted in excess onshore transport, which is consistent with results of others using a similar transport formula (Grunnet et al., 2004; Nienhuis et al., 2016; Hopkins et al., 2018). The excess onshore transport using default parameters is likely related to the parameterization of the transformation of wave shape into shallow water and associated wave orbital velocity skewness and asymmetry in Delft3D (Albernaz et al., 2019). By reducing the transport parameters SusW and BedW each to 0.2 (20% of the default value), our simulations were able to reproduce the rate of dispersion of berm sediment out of the survey area and onshore movement of the berm centroid (Figs. 6 and 7; Table 3). Albernaz et al. (2019) suggested that the reduction of these transport parameters may have unintended consequences, including underestimation of alongshore transport rates outside of the observed area. However, our sensitivity analysis suggested that variations in transport parameters more strongly affected the cross-shore sediment flux than the alongshore component (Fig. 5D–F). Regardless, future work should investigate the effect of alternate parameterizations to characterize wave transformation, wave orbital skewness, and asymmetry (e.g., Ruessink et al., 2012) on predictions of berm transport and morphology.

Sensitivity analysis suggested variations in transport coefficients and the thickness of bed layering controlled the magnitude of onshore sediment flux from the berm in a similar manner (Fig. 5A–F). Thicker bed layers and lower transport coefficients led to less onshore transport and only indirectly affected the alongshore dispersal. For simulations with lower onshore sediment flux, less sediment reached the surf zone. On the other hand, variations in grain size altered not only the magnitude but the pathways of sediment transport (Fig. 5G–I). In contrast to berms composed of coarser sediment, the berm with a median diameter of 0.15 mm was largely transported as suspended load and directed mostly alongshore. These results suggest preferential transport of coarser sediment particles onshore while finer particles are transported alongshore and more likely retained on the outer ebb delta. While not included in these model simulations, actual grain size distributions vary spatially in the mouth of the Columbia River and ebb tidal delta (Sherwood and Creager, 1990) and likely contribute to more complex patterns of sediment transport around the ebb delta. The effects of spatially variable sediment grain size distributions on sediment transport rates (e.g., Huisman et al., 2018) and dispersion of berm sediment should be considered in future model applications.

5.3. Berm performance

A primary goal of the berm placement, monitoring, and numerical modeling performed in this study was to evaluate the rates of sediment transport and potential to enhance the sediment supply onshore to locally eroding beaches from the North Head Site prior to operational use in a broader regional sediment management program. In particular, the establishment of the dredge placement site on the north side of the mouth of the Columbia River was intended to provide additional sediment to Benson Beach, a 3-km stretch of coast between the Columbia River North Jetty and North Head that eroded more than 2 Mm^3 of sediment between 2014 and 2019 (Stevens et al., 2020). Observations and model predictions of berm morphology suggest that sediment placed in the southern portion of the North Head Site, where the berm was located, erodes and transport is primarily onshore (Figs. 4–7). With generally weak near-bed tidal currents (Fig. 3), transport events at this location were episodic and initiated primarily due to wave enhanced bottom stresses and wave driven currents (Fig. 8). Sediment from the berm was initially transported onshore and eventually incorporated into the surf zone, but the transport pathway between berm and onshore beaches was sensitive to variations in wave direction (Fig. 9). Waves from the west moved sediment in northeasterly direction and sediment from the berm was predicted to by-pass Benson Beach and accumulate north of North Head (Fig. 9*E*). Waves from the northwest induce onshore transport from the berm and southerly transport in the surf zone, resulting in sediment accumulation along Benson Beach (Fig. 9F).

The model simulations that best predicted the observed morphologic change of the berm (R1, R5; Table 3) indicate that between 9 and 17% of the initial measured volume (204,000 m^3) in the berm accumulated along Benson Beach during the 169-day hindcast (Fig. 10). Continued accumulation of sediment at the end of the simulations suggests that the berm would likely continue to enhance the sediment supply of Benson Beach as more sediment erodes from the berm and is transported onshore. Regardless, much larger quantities of dredge material placed within the North Head Site will be required during operational use to reverse the erosional trend at Benson Beach given the large deficit in sediment supply (about 440,000 m^3/yr between 2014 and 2019; Stevens et al., 2020) and the relatively modest efficiency of transport between the North Head Site and the beach.

5.4. Regional sediment management at the mouth of the Columbia river

Between 2 and 4 Mm^3 of sediment is dredged from the navigation channel at the mouth of the Columbia River annually (USACE, 2021). Dredging usually takes place between August and October depending on vessel availability and weather conditions. Sediment is preferentially placed in nearshore sites and disposal in deep water is limited to reduce loss of sediment from the littoral system. The location of the North Head Site was selected to accompany two other oceanic shallow water dredge placement areas (Shallow Water and South Jetty Sites) as well as the deep-water disposal area (Deep Water Site) that are currently used to place sediment dredged from the navigation channel (Fig. 1). The operational strategy for the nearshore sites employs “thin layer” placement whereby dredged sediment is distributed evenly over the site to control excess sediment accumulation, limit wave amplification, and to reduce impacts on benthic organisms (Roegner et al., 2021). The sites are adaptively managed during dredging operations and repeat bathymetric surveys are used to identify capacity within specific areas in the nearshore sites. In 2020, 216,000 m^3 of sediment was placed in the North Head Site to form the nearshore berm, 1.3 Mm^3 was placed in the Shallow Water Site, 306,000 m^3 was placed within South Jetty Site, and 274,000 m^3 was disposed of in the Deep Water Site. These volumes are comparable to the sediment deficit and observed erosion on adjacent beaches (Stevens et al., 2020), indicating that efficient strategic nearshore placements can reduce or potentially reverse the observed erosion trends.

Quantitative comparisons of the rates of dispersion and fate of sediment placed within the nearshore sites are used to inform effective regional sediment management. Model scenarios that included hypothetical berms in current operational placement areas indicate that sediment placed within the newly established North Head Site will disperse at similar rates to those at the South Jetty Site (Fig. 11). This suggests that the North Head Site is suitable for annual, thin-layer placement of sediment dredged to maintain the Columbia River navigation channel. Similar procedures employed for management of the South Jetty Site, which have been tested over years of use and vetted with stakeholders concerned with potential negative impacts of dredged material placement on benthic resources and navigational safety, are appropriate for operational placement at the North Head Site. Both the North Head Site and the South Jetty Site are much less dispersive than the Shallow Water Site. In scenarios investigating alternative berm placement locations, roughly 50% of the sediment placed within the North Head and South Jetty Sites remained within the original footprint of the berm during the 169-day study period while the entire berm placed within Shallow Water Site was dispersed as early as January 2021 (Fig. 11). The main difference between Shallow Water Site and the other nearshore placement sites is the presence of strong tidal currents in the vicinity of the inlet with near-bed currents predicted to regularly exceed 1 m/s. The high rate of sediment dispersion allows for much larger quantities of sediment to be placed within Shallow Water Site without exceeding capacity. Sediment placed in the Shallow Water Site enhances the sediment supply to the beaches north of the inlet (Fig. 11D), though not as efficiently as the North Head Site over the interval of the hindcast simulation. Most of the sediment placed in the Shallow Water Site initially was transported offshore onto the ebb delta. After initial offshore transport, sediment originally placed in the Shallow Water Site moved onshore and accumulated along Benson Beach (Fig. 11D). Of the scenarios investigated in this study, the actual berm location in the southern portion of North Head Site was most efficient at delivering sediment to Benson Beach.

6. Conclusions

A combination of field measurements and numerical modeling was used to improve understanding and prediction of coastal processes, as well as to inform regional sediment management at the mouth of the Columbia River, USA. Repeated multibeam bathymetric surveys quantified the initial morphology and subsequent dispersion of a nearshore berm composed of 216,000 m^3 of sand-sized sediment dredged from the navigation channel and placed in water depths between 12 and 15 m on the northern flank of the ebb-tidal delta. Throughout the monitoring

period between September 22, 2020, and March 10, 2021, the broad, low relief berm thinned by 60% and the volume decreased by 40% as it dispersed primarily in the onshore direction.

The observations of berm morphology were used to calibrate a three-dimensional hydrodynamic and sediment transport model. Poorly constrained model inputs including transport coefficients, bed schematization, and grain size were refined based on comparisons between modeled and observed berm morphology. The areal extent, mean thickness, and displacement of the berm centroid were most sensitive to the bed schematization – in particular, the thickness of the transport- and under-layers used to represent bed stratigraphy in the model. The volume of the berm within the survey area was controlled primarily by sediment transport coefficients related to wave asymmetry. The default values of the transport coefficients resulted in excessive onshore transport and were reduced by 80% during calibration. Variations in grain size altered not only the magnitude of berm dispersion but also the pathway, with finer sands preferentially transported in the alongshore direction. The calibrated model was largely able to reproduce the observed change in berm morphology including the timing and magnitude of volume loss within the survey area, spreading, thinning, and onshore movement of the berm centroid. Careful consideration of these model inputs should therefore be taken to accurately simulate transport of sand-sized sediment in energetic, open-coast settings.

A modeling methodology was developed that allowed for the quantification of sediment transport rates and identification of the dominant processes responsible for the dispersal of berm sediment following placement. Wave enhanced shear stresses and asymmetry in wave orbital motions were the primary process controlling the onshore dispersion of the berm. Between 9 and 17% of the initial volume of the berm was predicted to accumulate along the shoreface of a shoreline reach experiencing chronic erosion during the study period. Observations and model results indicate that the berm location is suitable for strategic placement of sediment as part of a larger, operational regional sediment management program. The transferrable monitoring and modeling framework developed here suggests that strategic placement of dredged sediment in the active nearshore is a viable technique to consider for enhancement of sediment supplies in high energy coastal environments.

Author credit statement

Andrew Stevens: Conceptualization, Methodology, Writing-Original Draft, Writing-Review and Editing **Hans Moritz:** Conceptualization, Methodology, Project administration, Writing – Review and Editing **Edwin Elias:** Methodology, Writing – Review and Editing **Guy Gelfenbaum:** Conceptualization, Funding acquisition, Writing – Review and Editing **Peter Ruggiero:** Writing – Review and Editing **Stuart Pearson:** Methodology, Writing – Review and Editing **James McMillan:** Conceptualization, Project administration, Funding acquisition, Writing – Review and Editing **George Kaminsky:** Conceptualization, Writing – Review and Editing.

Declaration of competing interest

The authors declare that they have no known competing financial interests or personal relationships that could have appeared to influence the work reported in this paper.

Data availability

Processed multibeam bathymetry datasets and hydrodynamic and sediment transport model input files suitable for use with Delft3D version 4.04.01 are available in Stevens et al. (2023). Time series oceanographic observations used for model validation will be made available on request.

Acknowledgments

We thank the captain and crew of the U.S. Army Corps of Engineers (USACE) dredge *Essayons* who performed the dredged material placement to construct the nearshore berm and the USACE Portland District Surveys Section for acquiring the bathymetric data used in this study. Funding was provided by the USACE, Portland District, and U.S. Geological Survey (USGS) Coastal and Marine Hazards and Resources Program. We thank Katherine Groth and Julia Keiter (USACE) for project coordination, Bert Jagers (Deltares) for helpful discussions about sediment transport modeling, and Charles Seaton (Center for Coastal Margin Observation and Prediction) for assistance accessing meteorological observations. Members of the Lower Columbia Solutions Group provided valuable feedback and encouragement throughout this study. Reviews by Jon Warrick (USGS) and two anonymous reviewers greatly improved an earlier version of this manuscript. Any use of trade, firm, or product names is for descriptive purposes only and does not imply endorsement by the U.S. Government.

References

Ahn, S., Neary, V.S., Haas, K.A., 2022. Global wave energy resource classification system for regional energy planning and project development. Renew. Sustain. Energy Rev. 162, 112438 https://doi.org/10.1016/j.rser.2022.112438.

Akan, C., Moghimi, S., Ozkan-Haller, H.T., Osborne, J., Kurapov, A., 2017. On the dynamics of the Mouth of the Columbia River: results from a three-dimensional fully coupled wave-current interaction model. J. Geophys. Res. Ocean. 122, 5218–5236.

Albernaz, M.B., Ruessink, G., Jagers, H.R.A., Kleinhans, M.G., 2019. Effects of wave orbital velocity parameterization on nearshore sediment transport and decadal morphodynamics. J. Mar. Sci. Eng. 188 https://doi.org/10.3390/jmse7060188.

Allan, J.C., Gabel, L.L., 2016. Monitoring the Response and Efficacy of a Dynamic Revetment Constructed Adjacent to the Columbia River South Jetty, Clatsop County, Oregon. Oregon Department of Geology and Mineral Industries Open-File Report, p. 50. O-16-07.

Allen, R.C., Lacy, J.R., Stevens, A.W., 2021. Cohesive sediment modeling in a shallow estuary: model and environmental implications of sediment parameter variation. J. Geophys. Res. Ocean. 126 https://doi.org/10.1029/2021JC017219.

Baptist, M.J., Gerkema, T., van Prooijen, B.C., van Maren, D.S., van Regteren, M., Schulz, K., Colosima, I., Vroom, J., van Kessel, T., Grasmeijer, B., Willemsen, P., Elschot, K., de Groot, A.V., Cleveringa, J., van Eekelen, E.M.M., Schuurman, F., de Lange, H.J., van Puijenbroek, M.E.B., 2019. Beneficial use of dredged sediment to enhance salt marsh development by applying a 'Mud Motor. Ecol. Eng. 127, 312–323.

Bertin, X., Mengual, B., de Bakker, A., Guerin, T., Martins, K., Pezert, M., Lavaud, L., 2020. Recent advances in tidal inlet morphodynamic modelling. J. Coast Res. 95, 1016–1020.

Blaylock, B.K., Horel, J.D., Liston, S.T., 2017. Cloud archiving and data mining of high resolution rapid refresh model output. Comput. Geosci. 109, 43–50.

Booij, N., Ris, R.C., Holthuijsen, L.H., 1999. A third-generation wave model for coastal regions, Part I—model description and validation. J. Geophys. Res. 104, 7649–7666.

Bosboom, J., Reniers, A.J.H.M., 2014. Displacement-base error metrics for morphodynamic models. Adv. Geosci. 39, 37–43.

Brutsche, K.E., Wang, P., Beck, T.M., Rosati, J.D., Legault, K.R., 2014. Morphological evolution of a submerged artificial nearshore berm along a low-wave microtidal coast, Fort Myers Beach, west-central Florida, USA. Coast. Eng. 91, 29–44.

de Schipper, M.A., Ludka, B.C., Raubenheimer, B., Luijendijk, A.P., Schlacher, T.A., 2021. Beach nourishment has complex implications for the future of sandy shores. Nat. Rev. Earth Environ. 2, 70–84.

Deltares, 2018. Delft3D-Flow User Manual Version 3, 15, p. 672.

Egbert, G.D., Erofeeva, S.Y., 2002. Efficient inverse modeling of barotropic ocean tides. J. Atmos. Ocean. Technol. 19, 183–204.

Elias, E.P.L., Gelfenbaum, G., 2009. Modeling processes controlling sediment transport at the mouth of the Columbia River. Proc. Coast. Dynamic. https://doi.org/10.1142/9789814282475_0070, 2009, Paper No. 68.

Elias, E.P.L., Gelfenbaum, G., Wan der Westhuysen, A.J., 2012. Validation of a coupled wave-flow model in a high-energy setting: the mouth of the Columbia River. J. Geophys. Res. 117, C09011.

Elko, N., Roberts Briggs, T., Benedet, L., Robertson, Q., Thomson, G., Webb, B.M., Garvey, K., 2021. A century of U.S. beach nourishment. Ocean Coast Manag. 199, 105406 https://doi.org/10.1016/j.ocecoaman.2020.105406.

Fredsøe, J., 1984. Turbulent boundary layer in wave-current interaction. J. Hydraul. Eng. 110, 1103–1120.

French, J., Payo, A., Murray, B., Orford, J., Eliot, M., Cowell, P., 2016. Appropriate complexity for the prediction of coastal and estuarine geomorphic behaviour at decadal to centennial scales. Geomorphology 256, 3–16.

Gailani, J., Brutsche, K.E., Godsey, E., Wang, P., Hartman, M.A., 2019. Strategic Placement for Beneficial Use of Dredged Material. U.S. Army Engineer Research and Development Center. ERDC/CHL SR-19-3.

Gelfenbaum, G.R., Finlayson, D.P., Dartnell, P., Carlson, E., Stevens, A.W., 2015. Bathymetry and Backscatter from 2013 Interferometric Swath Bathymetry Systems

Survey of Columbia River Mouth, Oregon and Washington. U.S. Geological Survey data release. https://doi.org/10.5066/F7T72FHB.
Grasso, F., Bismuth, E., Verney, R., 2021. Unraveling the impacts of meteorological and anthropogenic changes on sediment fluxes along an estuary-sea continuum. Sci. Rep. 11, 20230 https://doi.org/10.1038/s41598-021-99502-7.
Grunnet, N.M., Walstra, D.J.R., Ruessink, B.G., 2004. Process-based modelling of a shoreface nourishment. Coast. Eng. 51, 581–607.
Hopkins, J., Elgar, S., Raubenheimer, B., 2018. Storm impact on morphological evolution of a sandy inlet. J. Geophys. Res. Ocean. 123, 5751–5762. https://doi.org/10.1029/2017JC013708.
Houston, J.R., Dean, R.G., 2016. Erosional impacts of modified inlets, beach encroachment, and beach nourishment on the east coast of Florida. J. Coast Res. 32, 227–240.
Huisman, B.J.A., Ruessink, B.G., de Schipper, M.A., Luijendijk, A.P., Stive, M.J.F., 2018. Modelling of bed sediment composition changes at the lower shoreface of the Sand Motor. Coast. Eng. 132, 33–49.
Huisman, B.J.A., Walstra, D.J.R., Radermacher, M., de Schipper, M.A., Ruessink, B.G., 2019. Observations and modelling of shoreface nourishment behavior. J. Mar. Sci. Eng. 7, 59. https://doi.org/10.3390/jmse7030059.
Kaminsky, G.M., Ruggiero, P., Buijsman, M.C., McCandless, D., Gelfenbaum, G., 2010. Historical evolution of the Columbia River littoral cell. Mar. Geol. 273, 96–126.
Karna, T., Baptista, A.M., Lopez, J.E., Turner, P.J., McNeil, C., Sanford, T.B., 2015. Numerical modeling of circulation in high-energy estuaries: a Columbia River estuary benchmark. Ocean Model. 88, 54–71.
Lesser, G.R., 2009. An Approach to Medium Term Coastal Morphological Modelling. Delft Technical University, Ph.D. Dissertation, Delft, Netherlands, p. 239.
Lesser, G.R., Roelvink, J.A., van Kester, J.A.T.M., Stelling, G.S., 2004. Development and validation of a three-dimensional morphological model. Coast. Eng. 51, 883–915.
Li, H., Beck, T.M., Moritz, H.R., Groth, K., Puckette, T., Marsh, J., Sanches, A., 2019. Sediment tracer tracking and numerical modeling at Coos Bay Inlet, Oregon. J. Coast Res. 35, 4–25.
Love, M.R., Friday, D.Z., Grothe, P.R., Carignan, K.S., Eakins, B.W., Taylor, L.A., 2012. Digital Elevation Model of Astoria, Oregon—Procedures, Data Sources and Analysis: National Oceanic and Atmospheric Administration. National Geophysical Data Center, p. 30.
Lower Columbia Estuary Partnership, 2010. Lower Columbia River Digital Terrain Model: Lower Columbia Estuary Partnership Website. https://www.estuarypartnership.org/lower-columbia-digital-terrain-model.
Ludka, B.C., Guza, R.T., O'Reilly, W.C., Merrifield, M.A., Flick, R.E., Bak, A.S., Hesser, T., Bucciarelli, R., Olfe, C., Woodward, B., Boyd, W., Smith, K., Okihiro, M., Grenzeback, R., Parry, L., Boyd, G., 2019. Sixteen years of bathymetry and waves at San Diego beaches. Sci. Data 6, 161. https://doi.org/10.1038/s41597-019-0167-6.
Luijendijk, A.P., Ranasinghe, R., de Schipper, M.A., Huisman, B.A., Swinkels, C.M., Walstra, D.J.R., Stive, M.J.F., 2017. The initial morphological response of the Sand Engine: a process-based modelling study. Coast. Eng. 119, 1–14.
MacMahan, J., 2016. Observations of oceanic-forced subtidal elevations in a convergent estuary. Estuar. Coast Shelf Sci. 181, 319–324.
Mendes, D., Pais-Barbosa, J., Baptista, P., Silva, P.A., Bernardes, C., Pinto, C., 2021. Beach response to a shoreface nourishment (Aveiro, Portugal). J. Mar. Sci. Eng. 9, 1112. https://doi.org/10.3390/jmse9101112.
Nienhuis, J.H., Ashton, A.D., Nardin, W., Fagherazzi, S., Giosan, L., 2016. Alongshore sediment bypassing as a control on river mouth morphodynamics. J. Geophys. Res.: Earth Surf. 121, 664–683. https://doi:10.1002/2015JF003780.
Pearson, S.G., van Prooijen, B.C., Elias, E.P.L., Vitousek, S., Wang, Z.B., 2020. Sediment connectivity: a framework for analyzing coastal sediment transport pathways. J. Geophys. Res.: Earth Surf. 125, e2020JF005595 https://doi.org/10.1029/2020JF005595.
Pearson, S.G., van Prooijen, B.C., Poleykett, J., Wright, M., Black, K., Wang, Z.B., 2021. Tracking fluorescent and ferromagnetic sediment tracers on an energetic ebb-tidal delta to monitor grain size-selective dispersal. Ocean Coast Manag. 212, 105835 https://doi.org/10.1016/j.ocecoaman.2021.105835.
Roegner, G.C., Fields, S.A., Henkel, S.K., 2021. Benthic video landers reveal impacts of dredged sediment deposition events on mobile epifauna are acute but transitory. J. Exp. Mar. Biol. Ecol. 538, 151526 https://doi.org/10.1016/j.jembe.2021.151526.
Roelvink, D., Huisman, B., Elghandour, A., Ghonim, M., Reyns, J., 2020. Efficient modeling of complex sandy coastal evolution at monthly to century time scales. Front. Mar. Sci. https://doi.org/10.3389/fmars.2020.00535.
Rogers, W.E., Babanin, A.V., Wang, D.W., 2012. Observation-consistent input and whitecapping dissipation in a model for wind-generated surface waves: description and simple calculations. J. Atmos. Ocean. Technol. 29, 1329–1346.
Ruessink, B., Ramaekers, G., van Rijn, L., 2012. On the parameterization of the free-strem non-linear wave orbital motion in nearshore morphodynamic models. Coast. Eng. 65, 56–63.
Ruggiero, P., Komar, P.D., Allan, J.C., 2010. Increasing wave heights and extreme value projections—the wave climate of the U.S. Pacific Northwest. Coast. Eng. 57, 539–552.
Ruggiero, P., Kaminsky, G.M., Gelfenbaum, G., Cohn, N., 2016. Morphodynamics of prograding beaches—a synthesis of seasonal- to century-scale observations of the Columbia River littoral cell. Mar. Geol. 376, 51–68.
Schlacher, T.A., Noriega, R., Jones, A., Dye, T., 2012. The effects of beach nourishment on benthic invertebrates in eastern Australia: impacts and variable recovery. Sci. Total Environ. 435–436, 411–417. https://doi.org/10.1016/j.scitotenv.2012.06.071.
Sherwood, C.R., Creager, J.S., 1990. Sedimentary geology of the Columbia River estuary. Prog. Oceanogr. 25, 15–79.
Stevens, A.W., Gelfenbaum, G., Ruggiero, P., Kaminsky, G.M., 2012. Southwest Washington Littoral Drift Restoration: Beach and Nearshore Morphological Monitoring, 1175. US Geological Survey Open-File Report 2012-, p. 67. https://doi.org/10.3133/ofr20121175.
Stevens, A.W., Weiner, H.M., Wood, J.M., Ruggiero, P., Kaminsky, G.M., Gelfenbaum, G. R., 2019. Beach Topography and Nearshore Bathymetry of the Columbia River Littoral Cell, Washington and Oregon (Ver. 3.0, December 2021). U.S. Geological Survey data release. https://doi.org/10.5066/P9W15JX8.
Stevens, A.W., Elias, E., Pearson, S., Kaminsky, G.M., Ruggiero, P.R., Weiner, H.M., Gelfenbaum, G.R., 2020. Observations of coastal change and numerical modeling of sediment-transport pathways at the mouth of the Columbia River and its adjacent littoral cell. U.S. Geological Surv. Open-File Rep. 2020 1045, 82. https://doi.org/10.3133/ofr20201045.
Sutherland, J., Peet, A.H., Soulsby, R.L., 2004. Evaluating the performance of morphological models. Coast. Eng. 51, 917–939.
U.S. Geological Survey, 2021. National water information system: U.S. Geological survey web interface. Cited May 2021 at. https://doi.org/10.5066/F7P55KJN. https://nwis.waterdata.usgs.gov/nwis.
USACE, 2021. 2021 Annual Use Plan. Management of Open Water Dredged Material Placement/disposal Sites. U.S. Army Corps of Engineers Portland District, Mouth of the Columbia River, OR and WA, p. 120.
van der Wegen, M., Dastgheib, A., Jaffe, B.E., Roelvink, D., 2011. Bed composition generation for morphodynamics modeling: case study of San Pablo Bay in California, USA. Ocean Dynam. 61, 173–186.
Van Prooijen, B.C., Tissier, M.F., De Wit, F.P., Pearson, S.G., Brakenhoff, L.B., Van Maarseveen, M.C., De Looff, H., 2020. Measurements of hydrodynamics, sediment, morphology and benthos on Ameland ebb-tidal delta and lower shoreface. Earth Syst. Sci. Data 12, 2775–2786.
Van Rijn, L.C., 1993. Transport of fine sands by currents and waves. J. Waterw. Port, Coast. Ocean Eng. 119, 123–143.
Van Rijn, L.C., 1993a. Principles of Sediment Transport in Rivers, Estuaries, and Coastal Seas. Aqua Publications, Delft, Netherlands.
Verboom, G.K., Slob, A., 1984. Weakly-reflective boundary conditions for two-dimensional shallow water flow problems. Adv. Water Resour. 7, 192–197.
Willmott, C.J., 1982. Some comments on the evaluation of model performance. Bull. Am. Meteorol. Soc. 63, 1309–1313.
Xu, J., Myers, E., White, S., 2010. VDatum for the Coastal Waters of North/Central California, Oregon and Western Washington—Tidal Datums and Sea Surface Topography, 22. National Oceanic and Atmospheric Administration Technical Memorandum NOS CS, p. 68.
Yates, M.L., Guza, R.R., O'Reilly, W.C., Seymour, R.J., 2009. Seasonal persistence of a small southern California beach fill. Coast. Eng. 56, 559–564.

Further reading

Stevens, A.W., Moritz, H.R., McMillan, J.M., 2023. Bathymetry Data and Sediment Transport Modeling of a Submerged Nearshore Berm at the Mouth of the Columbia River. U.S. Geological Survey data release, Washington. https://doi.org/10.5066/P9RVK9S9.